

Numerical investigation of highly excited magnetic monopoles in $SU(2)$ Yang-Mills–Higgs theory

Gyula Fodor and István Rácz^y
*MTA KFKI, Részecske- és Magfizikai Kutatóintézet
 H-1121 Budapest, Konkoly Thege Miklós út 29-33.
 Hungary*

(Dated: December 24, 2018)

Preliminary results concerning the time evolution of strongly excited $SU(2)$ Bogomolny-Prasad-Sommerfield (BPS) magnetic monopoles have been published in [11]. The behavior of these dynamical magnetic monopoles was investigated by means of numerical simulations in the four dimensional Minkowski spacetime. The developed code incorporates both the techniques of conformal compactification and that of the hyperboloidal initial value problem. Our primary aim here is to provide a detailed account on the methods and results of the investigations reported in [11]. In addition, some important new results, which go much beyond the scope of these early studies, are also presented.

PACS numbers: 03.50.Kk, 14.80.Hv

I. INTRODUCTION

Soliton and quasi-soliton type configurations, which are in general spatially localized non-singular finite energy solutions of non-linear field equations, play significant role in various particle physics considerations (see e.g. [22, 28] for recent reviews). In general the associated field equations are highly non-linear, therefore, most of the investigations have been restricted to the study of time independent configurations. Thereby, there is an obvious increase of interest to study the dynamical properties of soliton type configurations. It is a matter of fact that the available analytic techniques either have not been developed enough to provide or simply cannot guarantee completely satisfactory answers to all questions in case of non-linear systems. Therefore, reliable numerical approaches are needed which are able to describe the time evolution of these type of systems. Motivated by this sort of necessities we have developed a numerical method which have been used in studying the time evolution of various spherically symmetric non-linear dynamical systems [9, 10, 11, 12] (see also [4]). This numerical method is based on the “method of lines” in a fourth order setting [16] which was found to be the most efficient among the numerical methods which are applied in various considerations [18]. In addition, to get a faithful representation of all the radiation processes the techniques of conformal compactification (introduced first by Penrose [25]) to the underlying Minkowski spacetime, along with the hyperboloidal initial value problem were also incorporated. The applied conformal gauge, which is a modification of the static hyperboloidal gauge makes it possible to inves-

tigate by numerical means the asymptotic properties of radiation processes. One of the associated advantages is that by making use of this method the radiation processes, which last infinitely long in physical time, can be analyzed in finite computational time intervals.

Among the great variety of physically interesting soliton type configurations distinguished attention has been paid to the study of magnetic monopole type configurations such as the 't Hooft-Polyakov magnetic monopole solutions of coupled Yang-Mills–Higgs (YMH) systems [26]. However, even in the case of magnetic monopoles there was a lack of knowledge concerning the dynamical properties of these systems. Therefore, our numerical method was first applied to the study of the dynamical properties of the simplest possible magnetic monopole system, which could be chosen so that there was a radiative component among the basic field variables. This paper is, in fact, to report about the results of investigations concerning the time evolution of a strongly excited spherically symmetric $SU(2)$ BPS magnetic monopole [2].

To have a clear enough setting from the energetic point of view we investigated the time evolution of an initially static $SU(2)$ BPS magnetic monopole which was excited by the help of a high energy pulse. The self-interaction of the Higgs field was turned off which yielded a Yang-Mills–Higgs system so that the Yang-Mills field is massive while the Higgs field is massless.

The dynamics started by injecting a pulse of excitation via the time derivative of the Yang-Mills variable. Since the Yang-Mills and Higgs variables are coupled (in a non-linear manner) energy was transformed to the massless Higgs field which immediately forwarded about half of the energy of the pulse towards future null infinity, \mathcal{I}^+ . Naively, one would expect that the following part of the evolution is going to be quite boring since only a lower scale energy transform will happen until the rest of the energy of the exciting pulse

Electronic address: gfodor@rmki.kfki.hu

^yElectronic address: iracz@sunserv.kfki.hu

disperse and the system settles down to the static monopole.

Contrary to this simple scenario quite interesting features of the underlying non-linear system show up. First of all the exciting pulse seems to leave the central region so that it sweeps out some part of the energy of the original static monopole from that region together with itself. Such a process is clearly justified by the fact that in the central region, where a long-lasting quasi-stable 'breathing state' develops, the average energy density seems to be always less than that of the static monopole was. Since the original static magnetic monopole is stable we know that by the end the missing energy has to come back to the central region. However, as our numerical simulations indicates [11] this process is unexpectedly slow and, in certain cases, behaves completely contrary to our expectations. For instance, the difference between the dynamical and the original static energies contained in a ball of radius r may be positive or negative depending on the strength of the non-linear aspects of the dynamics, as well as, on location, i.e. on the value of r . Nevertheless, a distant observer, say from a distance ten times larger than the characteristic size of the original monopole, will see a power law decrease of this difference of energies in time approximately with power $3=2$.

In the meantime the energy is getting to be stored in expanding shells of oscillations of the massive Yang-Mills field built up in the distant region. These shells of oscillations behaves much like the oscillations of a simple massive Klein-Gordon field (see for a detailed investigation [10]) since the coupling of the Yang-Mills and Higgs variables is negligible there. The monopole can pull back the missing energy to build up the quasi-static configuration in the central region only very slowly.

Due to the coupling of the Yang-Mills and Higgs fields in the central region the massless Higgs field continuously take away a small fragment of the energy of the "breathing" monopole, which is radiated to future null infinity. The corresponding decrease of the total energy which can be associated with the hyperboloidal hypersurfaces decreases in time with power $5=3$.

Note, however, that this total energy, as well as, its limit value, is always strictly larger than the energy of the original static monopole. This is because the expanding shells of oscillations store some part of the energy of the original pulse forever. In fact, this part of the energy cannot reach future null infinity since it is associated with the massive Yang-Mills field, moreover, as they are getting further and further away from the central region the monopole can get back less and less energy from them since non-linear effects are getting to be negligible.

The time evolution of the frequency of oscillations of the excited monopole behaves also somewhat counter to the general expectations. Instead of hav-

ing a slow decay in the frequency of these oscillations as their amplitude decreases there is an increase in the frequency which takes the maximum value in the asymptotic region, i.e. at future timelike infinity. Interestingly, while the frequency of the breathing monopole tends to the mass of the Yang-Mills field from below the frequency of the oscillations stored in the expanding shell has no upper bound, although the amplitude is decreasing, as in case of the massive Klein-Gordon field [10]. Note that these phenomenon are not at all unphysical. Recall that a simple physical system like the spinning coin on the desk can produce a quite similar effect. As energy loss happens due to dissipative processes the amplitude of the "spinning" is getting smaller and smaller in consequence of which the frequency of the oscillations is getting higher and higher. In case of the distant oscillating shells the unbounded increase of the frequency is, in fact, to compensate the decrease of the oscillation amplitudes which together ensure the conservation of the energy stored by the shells.

In virtue of these results it seems not to be overrating to say that the investigation of the dynamics properties of magnetic monopoles made transparent a number of interesting and unexpected features of the underlying non-linear system. Hopefully, these sort of investigations will stimulate further numerical and analytic investigations of various non-linear dynamical systems. For instance, partly motivated by the findings of the above described investigations, in a framework of linear perturbation theory some of the above mentioned features could be explained successfully both qualitatively and quantitatively [14]. Note, however, that truly non-linear effects are by their very nature out of the scope of these sort of investigations, in particular, as some of the new results of this paper make it transparent, they cannot be used to describe the behavior of the investigated system when the energy of the exciting pulse is much larger than that of the original static monopole.

The structure of this paper is as follows. In the next section, after recalling some of the basics related to the properties of the underlying generic dynamical system a detailed description of the specific choice for both the YMH system and the geometry is provided. The static hyperboloidal conformal gauge applied in our investigations is introduced in section III, while the first order representation of the field equations, relevant for this choice of conformal setting, is given in section IV. A detailed description of the applied numerical scheme is presented in section V, while various numerical tests of the code, for the case of massive and massless Klein-Gordon field, are presented in section VI. Finally, all the numerical results concerning the evolution of dynamical magnetic monopoles, including subsections providing detailed description of energy transfers, monitoring of the numerical violation of constraints and the energy conservation, along

with the behavior of the magnetic charge density, are presented in section VII.

II. PRELIMINARIES

The investigated dynamical magnetic monopole is described as a coupled $SU(2)$ YMH system. The Yang-Mills field is represented by an $su(2)$ -valued vector potential A_a and the associated 2-form field F_{ab} reads as

$$F_{ab} = \partial_a A_b - \partial_b A_a + ig [A_a; A_b] \quad (1)$$

where $[;]$ denotes the product in $su(2)$ and g stands for the gauge coupling constant. The Higgs field (in the adjoint representation) is given by an $su(2)$ -valued function while its gauge covariant derivative reads as $D_a = \partial_a + ig [A_a; \cdot]$. The dynamics of the investigated YMH system is determined by the action

$$S = \int d^4x [Tr(F_{ef}F^{ef}) + 2 Tr(\partial_e D^e) - V(\phi)] \quad (2)$$

where d^4x is the 4-dimensional volume element, moreover, $V(\phi)$, describing the self-interaction of the Higgs field, is chosen to be the standard quadratic potential

$$V(\phi) = \frac{1}{4} Tr(\phi^2) - H_0^2 \phi^2, \quad (3)$$

where ϕ and H_0 denote the Higgs self-coupling constant and the ‘vacuum expectation value’ of the Higgs field, respectively.

The symmetric energy-momentum tensor of the considered YMH system takes the form

$$T_{ab} = \frac{1}{4} Tr(F_{ae}F_b^e) - Tr(\partial_a D_b) + \frac{1}{4} g_{ab} L, \quad (4)$$

where L stands for the Lagrangian

$$L = Tr(F_{ef}F^{ef}) + 2 Tr(\partial_e D^e) - V(\phi). \quad (5)$$

A. Fixing the geometrical and gauge setup

This paper is to investigate the evolution of spherically symmetric Yang-Mills-Higgs (YMH) systems on a flat Minkowski background spacetime. Accordingly, as a fixed background, the four-dimensional Minkowski spacetime $(\mathbb{R}^4; \eta_{ab})$ will be applied, the line element of which in the conventionally used Descartes-type coordinates $(x^0; x^1; x^2; x^3)$ reads as

$$ds^2 = (dx^0)^2 - (dx^1)^2 - (dx^2)^2 - (dx^3)^2. \quad (6)$$

The gauge group is specified by giving the set of generators $f_I g$ ($I=1,2,3$) of the associated $su(2)$ Lie algebra which reads as

$$\epsilon_I = \frac{1}{2} \epsilon_I; \quad (7)$$

where ϵ_I denote the Pauli matrices. The commutation relations relevant for this choice of generators are

$$[\epsilon_I; \epsilon_J] = i \epsilon_{IJK} \epsilon_K; \quad (8)$$

where ϵ_{IJK} denotes the completely antisymmetric tensor with $\epsilon_{123} = 1$.

In addition to the above special choice concerning the gauge group, our considerations will be restricted to YMH systems which are yielded by the ‘minimal’ dynamical generalization of the static t’Hooft-Polyakov magnetic monopole configurations [17, 26] (see also [15, 19]). Accordingly, the Yang-Mills and Higgs field variables, $A_a = A_a^I \epsilon_I$ and $\phi = \phi^I \epsilon_I$, are specified, in the Coulomb gauge, via the relations

$$A_0^J = 0; \quad A_I^J = \frac{(1-w)}{g} \epsilon_{IJK} \frac{x^K}{r^2} \quad (9)$$

$$\phi^I = H \frac{x^I}{r}; \quad (10)$$

where the functions w and H are assumed to be smooth functions in \mathbb{R}^4 depending upon the coordinates $x^0; x^1; x^2; x^3$ only in the combinations $t = x^0$ and $r = \sqrt{(x^1)^2 + (x^2)^2 + (x^3)^2}$.

Since the metric, as well as the matter fields, are required to be spherically symmetric, the use of the standard coordinates $(t; r; \theta; \phi)$, adapted to the spherical symmetry of $(\mathbb{R}^4; \eta_{ab})$, is the most suitable. In these coordinates the line element of the Minkowski metric takes the form

$$ds^2 = dt^2 - dr^2 - r^2 d\theta^2 + \sin^2 \theta d\phi^2. \quad (11)$$

We have assumed above that w and H are smooth functions of t and r . This might be surprising especially because our eventual aim is to carry out numerical simulations of the YMH systems under considerations. Numerical methods are inherently too rough to make a sensible distinction between configurations belonging to different differentiability classes. In fact, our smoothness assumption is to ensure certain technical conveniences used later and it is supported by the following considerations. (Note that for the following argument it would be enough to assume that w and H are smooth in a sufficiently small neighborhood of the origin.) In numerical simulation of spherically symmetric configurations a grid boundary representing the origin inevitably appears. This means that we need to solve an initial-boundary value problem which, in particular, requires the specification of

'boundary behavior' of w and H at the origin throughout the time evolution. This is, in fact, the very point where we make use of our smoothness assumption. In virtue of (9) and (10) it is straightforward to see that spherical symmetry, along with the required smoothness of w and H through the origin, ensures that in a neighborhood of the origin w and H are even and odd functions of the r -coordinate, respectively. Consequently, as it is described in subsection V D in more detail, by extending our grid by a suitable number of virtual grid points the 'boundary values', for instance, of the r -derivatives of w and H need not be specified by hand instead they are naturally yielded by the time evolution of the corresponding odd and even functions.

The Yang-Mills field A_a as it is given by (9) is in the "Coulomb gauge". Another frequently used gauge representation is the so called "abelian gauge" in which has only one non-vanishing component, and which is achieved by making use of the gauge transformation

$$U = \exp(i\phi_2) \exp(i\phi_3); \quad (12)$$

A straightforward calculation yields that in the corresponding abelian gauge the Yang-Mills and the Higgs fields read as

$$A_a = \frac{1}{g} [w f_2(\phi_2) - \phi_1 \sin(\phi_2) g + \phi_3 \cos(\phi_2)] \quad (13)$$

and

$$= H_3; \quad (14)$$

The substitution of these gauge representations into the equations of motion, deducible from the action (2), yields the evolution equations for w and H which are given as

$$r^2 \partial_r^2 w - r^2 \partial_t^2 w = w - w^2 - 1 + g^2 r^2 H^2 \quad (15)$$

$$r^2 \partial_r^2 H + 2r \partial_r H - r^2 \partial_t^2 H = H - 2w^2 + \frac{1}{2} r^2 (H^2 - H_0^2); \quad (16)$$

The static finite energy solutions of these equations are called 't Hooft-Polyakov magnetic monopoles.

B. Regularity at the origin and at infinity

These equations, along with the former assumption concerning the smoothness of the basic variables, ensure certain regularity of the Yang-Mills and Higgs fields. In particular, it turned out that the values of w and H are restricted at the origin and at spacelike infinity throughout the evolution. At the origin (see appendix A for more details) the relations

$$w(t;0) = 1; \text{ and } H(t;0) = 0 \quad (17)$$

have to hold to have finite energy density, measured by the static observer with four velocity $u^a = (\partial_t, 0, 0, 0)$. In addition, whenever the smoothness of w and H is guaranteed in a neighborhood of the origin we also have

$$\partial_r^k w \Big|_{r=0} = 0 \quad (18)$$

for k being odd, while

$$\partial_r^k H \Big|_{r=0} = 0 \quad (19)$$

for k being even. For the first sight it might be a bit of surprise but a same type reasoning that lead to (18) and (19) provides a restriction also for the rest of the derivatives. Namely, from the field equations and from the smoothness requirement it follows that at the origin all the non-vanishing derivatives $\partial_r^k w$, with $k \geq 4$, and $\partial_r^k H$, with $k \geq 3$, can be given as a function of $\partial_r^2 w$ and $\partial_r^2 H$, along with their various time derivatives.

The argument associated with the regularity of the basic variables at spacelike infinity is more delicate. To get it we need to refer to the conformal (non-physical) setting, where our numerical simulation actually will be carried out. In this framework it seems to be essential to assume that the fields are at least C^2 even through future null infinity, I^+ . We refer here to this requirement as being merely a technical assumption, nevertheless, we would like to emphasize that the use of it is supported by the following observations. In [30] it was proved that the time evolution of a massive Klein-Gordon field in Minkowski spacetime with initial data of compact support necessarily yields $O(1=r^1)$ asymptotic behavior at null infinity. In addition, the results of Eardley and Moncrief [3, 7, 8, 23] concerning the local and global existence of YMH fields in 4-dimensional Minkowski spacetime supports that the above technical assumption can be deduced from the field equations at least in case of suitably chosen initial data specifications.

This smoothness requirement, along with the relevant form of the rescaled field equations, implies (see appendix A for more details) that w has to vanish while H has to be constant along the null geodesic generators of I^+ . The field equations also yield further restriction on this constant limit value H_1 of H at I^+ . In particular, H_1 must take the value H_0 whenever $\epsilon \neq 0$ but it is an arbitrary (positive) constant, C , otherwise. Thus, by making use of a limiting argument, the values of w and H at spacelike infinity can be seen to be determined as

$$w_1 = \lim_{r \rightarrow 1^-} w(t; r) = 0; \quad (20)$$

$$H_1 = \lim_{r \rightarrow 1^-} H(t; r) = \begin{cases} H_0; & \text{if } \epsilon \neq 0; \\ C; & \text{otherwise;} \end{cases} \quad (21)$$

Notice that the later relations are in accordance with our general expectations that the considered dynamical YMH systems do really possess the asymptotic

fall-off properties of a magnetic monopole [15, 19] throughout the time evolution.

It follows from equation (15), (16) and (21) that the semi-classical vector boson and Higgs mass, M_w and M_H , are

$$M_w = \frac{gH_1}{r} \quad (22)$$

$$M_H = \frac{p}{H_1} : \quad (23)$$

In particular, both fields are massless whenever H_1 vanishes, while only the Higgs field is massless, although it is coupled to a massive vector boson, whenever the self coupling constant g is zero.

Whenever the smoothness of the basic variables is guaranteed through I^+ then the n^{th} order r -derivatives of w and H are also restricted there. In particular, it follows from the relations (A.10), (A.15)-(A.18), along with the vanishing of the energy-momentum expressions at null infinity that whenever $H_1 \neq 0$ the asymptotic fall off conditions,

$$\lim_{r \rightarrow 1^-} r^{2n} \partial_r^n w(t; r) = 0 \quad (\text{for } n > 0) \quad (24)$$

and

$$\lim_{r \rightarrow 1^-} r^{2n} \partial_r^n H(t; r) = 0; \quad (\text{for } n > 2) \quad (25)$$

have to be satisfied.

It is important to note that whenever $g = 0$, i.e. the self-coupling of the Higgs field is turned down, there exists an explicitly known [27] static solution to (15) and (16)

$$w_s = \frac{gC r}{\sinh(gC r)} \quad (26)$$

$$H_s = C \frac{1}{\tanh(gC r)} - \frac{1}{gC r} ; \quad (27)$$

where C is an arbitrary positive constant which is in fact the limit value, H_1 , of the r.h.s. of (27). This static solution is called to be the Bogomolny-Prasad-Sommerfield (BPS) magnetic monopole which is known to be a linearly stable configuration [1].

Notice that in the BPS limit, i.e. whenever $g = 0$ and $H_1 = H_0 \neq 0$, the Higgs field becomes massless and the only scale parameter of the system is the vector boson mass $M_w = gH_1$. Since in the case considered here $H_1 \neq 0$, the re-scalings $t \mapsto tM_w$, $r \mapsto rM_w$ and $H \mapsto H/H_1$ transform the parameters to the value $g = H_1 = 1$. This implies that whenever we would like to study the excitations of the BPS monopole it suffices to consider the time evolution of the system only for the particular choice of the parameters $g = H_1 = 1$ because by inverse re-scalings of these solutions all the possible solutions to the field equations can be generated. Actually, to check the efficiency of our numerical implementation of the evolution equations first the stability of this

static solution was investigated. Later, the complete non-linear evolution of systems yielded by strong impulse type excitations of these analytic static solution was also studied in detail.

Although it is not necessary to be done, nevertheless we preferred to put the principal part of (16) into the same form as the principal part of (15) which was achieved by making use of the substitution

$$H(t; r) = \frac{h(t; r)}{r} + H_1 : \quad (28)$$

It follows then that our new basic variable h vanishes at the origin while it takes a finite limit value at infinity if H is guaranteed to tend to its boundary value fast enough there. The substitution of (28) into the relations (15) and (16) yields then

$$r^2 \partial_r^2 w \quad \partial_t^2 w = w \quad w^2 \quad 1 + g^2 (h + H_1 r)^2 \quad (29)$$

$$r^2 \partial_r^2 h \quad \partial_t^2 h =$$

$$(h + H_1 r) \quad 2w^2 + \frac{1}{2} (h^2 + 2H_1 r h) ; \quad (30)$$

where we have used the relation $H_1 = H_0$ whenever $g \neq 0$. The regularity of the solutions to these equations at $r = 0$ follows from the boundary conditions (17). It is important to note that (21) and (28), along with our smoothness and symmetry assumptions, which in particular implies that H is an odd function of r , guarantees that $h + H_1 r$ has to be an even function of the r -coordinate. Moreover, since $h^2 + 2H_1 r h = (h + H_1 r)^2 - H_1^2 r^2$ the right hand sides of (29) and (30) are both even functions of the r -coordinate. Notice finally that, by equations (29) and (30), the expressions $\partial_r^2 w \quad \partial_t^2 w$ and $\partial_r^2 h \quad \partial_t^2 h$ have regular limits at $r = 1$ because, in virtue of (21),(24),(25) and (28), w and h remain finite while r tends to infinity.

III. THE STATIC HYPERBOLOIDAL CONFORMAL GAUGE

In this section a conformal transformation of the Minkowski spacetime – along with the relevant form of the above matter field equations – will be considered.

The applied conformal transformation is a slightly modified version of the gauge transformation applied first by Moncrief [24] (see also [20]). It is defined by introducing the new coordinates $(T; R)$ instead of $(t; r)$ as

$$T(t; r) = \frac{t}{\sqrt{r^2 + 1}} \quad (31)$$

$$R(r) = \frac{1}{\sqrt{r^2 + 1}} \quad (32)$$

with the inverse relations

$$t = \frac{1}{R} \quad T + \frac{1 + R^2}{1 - R^2} \quad \text{and} \quad r = \frac{2R}{(1 - R^2)} ; \quad (33)$$

where α is an arbitrary positive constant. The Minkowski spacetime is covered by the coordinate domain satisfying the inequalities $-1 < T < +1$ and $0 < R < 1$ (see Fig.2).

The line element of the conformally rescaled metric $g_{ab} = \alpha^2 g_{ab}$ in coordinates $(T; R; \theta; \phi)$ takes the form

$$ds^2 = \frac{2}{2} dT^2 + 2R dT dR - dR^2 - R^2 d\theta^2 + \sin^2 \theta d\phi^2; \quad (34)$$

where the conformal factor is

$$\alpha(R) = \frac{1}{2}(1 - R^2); \quad (35)$$

and, by (33) and (35), we have the relation

$$r = R : \quad (36)$$

In this conformal representation the $R = 1$ coordinate line represents I^+ through which the metric g_{ab} smoothly extends to the coordinate domain with $R < 1$.

The name ‘static hyperboloidal gauge’ is explained by the following observations. First, (32) tells us that the $R = \text{const}$ lines represent world-lines of ‘static observers’, i.e. integral curves of the vector field $(\partial/\partial t)$. Second, it follows from (31) that the $T = \text{const}$ hypersurfaces are, in fact, hyperboloids satisfying the relation $(t - T)^2 - 2r^2 = 1$ in the Minkowski spacetime.

The equation describing radial null geodesics in the $(T; R)$ coordinate system is independent of the parameter θ ,

$$T = \frac{2R}{1 - R} + T_0; \quad (37)$$

with the plus signs corresponding to outgoing and the minus signs to ingoing geodesics. The form of the constant is chosen in a way that both type of geodesics cross the origin $R = 0$ at time $T = T_0$. The outgoing geodesic emanating from the origin reaches future null infinity $R = 1$ in a finite coordinate time at $T = T_0 + 1$. The ingoing geodesics starting from a point at radius R_0 at $T = 0$ reaches the origin at $T = 2R_0 = (1 - R_0)$. Consider now a geodesic starting at a point close to I^+ with radius $R_0 = 1 - R$. Such a geodesic reaches the origin at $T = -2 + 2 = R$. This means that for geodesics coming in from the far away region, the travel time essentially doubles when the geodesic starts from a point ‘twice as close’ to the $R = 1$ line. This has an important consequence in relation to the validity domain of our numerical code. Namely, the doubling of the resolution yields the doubling of the time interval within which we may expect our numerical simulation to provide a proper solution to the selected problem. Here it is assumed tacitly that all the possible inaccuracies born at and coming from

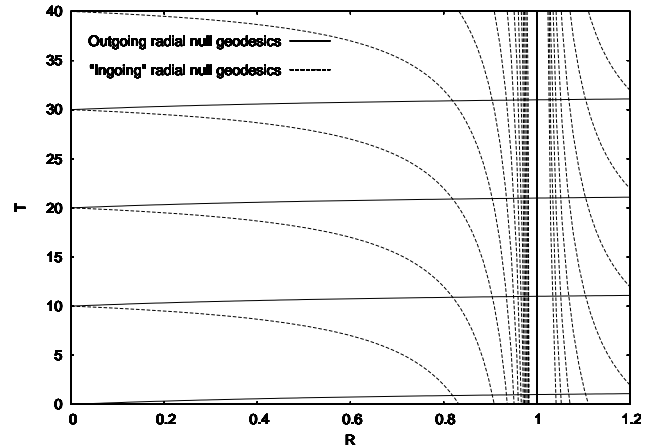


FIG. 1: The ingoing and outgoing radial null geodesic curves are shown in both the ‘physical’ and ‘unphysical’ regions. As in other conformal representations each point represents a two-sphere of radius R . The interior of the strip $0 < R < 1$ corresponds to the original Minkowski spacetime while I^+ is represented by the $R = 1$ coordinate line. Notice that the $R = \text{const}$ lines possesses timelike character everywhere except at the $R = 1$ line which is null.

the outer region – that is the part of the spacetime where the evolution cannot be described properly by any of the numerical techniques based on a finite grid – travel inwards only with the speed of light.

Consider now the field equations relevant for this conformal setting. To start off take a function $f = f(t; r)$ of the coordinates t and r and denote by $\mathbf{f} = \mathbf{f}(T; R)$ the function $f(t(T; R); r(T; R))$ yielded by the substitution of (33) into f . A straightforward calculation justifies then that for any pair of functions $f = f(t; r)$ and $\mathbf{f} = \mathbf{f}(T; R)$ the relation

$$r^2 \partial_r^2 f - \partial_t^2 f = \frac{4R^2}{(R^2 + 1)^2} - \frac{2}{2} \partial_R^2 \mathbf{f} - \partial_T^2 \mathbf{f} \quad (38)$$

$$2R \partial_R \partial_T \mathbf{f} - \frac{2}{(R^2 + 1)} \partial_T \mathbf{f} - \frac{R(R^2 + 3)}{(R^2 + 1)} \partial_R \mathbf{f}$$

holds. It follows then from (36) and (38) that the field equations, (29) and (30), in the current conformal representation read as

$$\frac{4R^2}{(R^2 + 1)^2} P \mathbf{v} = \mathbf{v} \cdot \mathbf{v}^2 - 1 + g^2 \mathbf{h} + H_1 R^{-1} \quad (39)$$

$$\frac{4R^2}{(R^2 + 1)^2} P \mathbf{h} = \mathbf{h} + H_1 R^{-1}$$

$$2\mathbf{v}^2 + \frac{1}{2} \mathbf{h} \cdot \mathbf{h} + 2H_1 R^{-1} \quad (40)$$

where the second order partial differential operator P is defined as

$$P = \frac{2}{2} \partial_R^2 - \partial_T^2 - 2R \partial_R \partial_T - \frac{2}{(R^2 + 1)} \partial_T \mathbf{f} - \frac{R(R^2 + 3)}{(R^2 + 1)} \partial_R \mathbf{f} : \quad (41)$$

As before, the regularity of the solutions to these equations at the origin, i.e. at $R = 0$ is guaranteed by the regularity of (29) and (30) at $r = 0$, while, the regularity at future null infinity, i.e. at $R = 1$, follows from (21), (24) and (25) provided that the fields have at least C^2 extensions through I^+ .

Hereafter, unless indicated otherwise, all the functions will be assumed to depend only on the coordinates T and R . Thereby we suppress all of the *tildes*, introduced above.

IV. THE FIRST ORDER HYPERBOLIC SYSTEMS

This section is to derive a first order hyperbolic system from the above evolution equations for which the initial value problem is well-posed. To see that equations (39) and (40) can be put into the form of a strongly hyperbolic system we shall follow a standard process (see e.g. [6]). Correspondingly first we introduce the first order derivatives of w and h ,

$$w_T = \mathcal{Q}_T w; \quad w_R = \mathcal{Q}_R w; \quad h_T = \mathcal{Q}_T h; \quad h_R = \mathcal{Q}_R h; \quad (42)$$

as new variables. In terms of the relevant enlarged set of dependent variables (39) and (40) can be given as

$$\theta_T w_T = -\frac{2}{2} (\theta_R w_R) - 2R (\theta_R w_T) + b_w \quad (43)$$

$$\mathcal{Q}_T h_T = -\frac{2}{2} (\mathcal{Q}_R h_R) - 2R (\mathcal{Q}_R h_T) + b_h; \quad (44)$$

where b_w and b_h are given as

$$b_w = -\frac{2}{(\mathbb{R}^2 + 1)} w_T \quad \frac{\mathbb{R}(\mathbb{R}^2 + 3)}{(\mathbb{R}^2 + 1)} w_R \quad (45)$$

$$b_n = \frac{2}{(R^2 + 1)} h_T - \frac{R(R^2 + 3)}{(R^2 + 1)} h_R + \frac{(R^2 + 1)^2}{4^2 R^2} (h + H_1 R) \quad (46)$$

It is straightforward to see that the above equations, along with the first and third equations of (42), and the integrability conditions

$$@_T w_R = @_R w_T \quad \text{and} \quad @_T h_R = @_R h_T; \quad (47)$$

possess the form of a first order system

$$\mathfrak{C}_T = A_{-B} (\mathfrak{C}_B) + B; \quad (48)$$

where α and B are given as

$$= \begin{matrix} 0 & 1 \\ w & \end{matrix} ; \quad B = \begin{matrix} 0 & 1 \\ w_T & \end{matrix} ; \quad (49)$$

moreover, A_R takes the form

$$A_R = \begin{matrix} 0 & 0 & 0 & 0 & 0 & 0 & 0 \\ 0 & 2R & 2 & 0 & 0 & 0 & 0 \\ 0 & 1 & 0 & 0 & 0 & 0 & 0 \\ 0 & 0 & 0 & 0 & 0 & 0 & 0 \\ 0 & 0 & 0 & 0 & 2R & 2 & A \\ 0 & 0 & 0 & 0 & 1 & 0 & 0 \end{matrix} \quad : \quad (50)$$

Since the eigenvectors of \mathbf{A}_R comprise a complete system and its eigenvalues are all real this first order system is, in fact, a strongly hyperbolic system [16].

Notice also that B does not depend on the space-like derivatives of ϕ , i.e. it is a functional of T , R and exclusively, $B = B(T; R)$. It is also straightforward to verify that the constraint equations, i.e. the second and the fourth equations of (42), are preserved by the time evolution governed by (48). This, in particular, guarantees that the pair of functions w and h yielded by the evolution of suitable initial data specifications will automatically satisfy the original evolution equations (39) and (40), as well, provided that the constraint equations hold on the initial data surface.

Finally, we would like to emphasize that the system specified by the relations (48) - (50) is not only strongly hyperbolic but can be put into the form of first order symmetric hyperbolic system. To see this introduce the variables \hat{w}_R and \hat{h}_R by the relations

$$\hat{w}_R = -w_R \quad \text{and} \quad \hat{h}_R = -h_R : \quad (51)$$

Then the system of field equations for the vector variable $\mathbf{u} = (\mathbf{w}; \mathbf{w}_T; \hat{\mathbf{w}}_R; \mathbf{h}; \mathbf{h}_T; \hat{\mathbf{h}}_R)^T$, possess the form of (48) with

$$A_R = \begin{matrix} 0 & 0 & 0 & 0 & 0 & 0 & 0 \\ 0 & 2R & = & 0 & 0 & 0 & 0 \\ 0 & 0 & = & 0 & 0 & 0 & 0 \\ 0 & 0 & 0 & 0 & 0 & 0 & 0 \\ 0 & 0 & 0 & 0 & 0 & 2R & = \\ 0 & 0 & 0 & 0 & = & 0 \end{matrix} \quad \begin{matrix} 1 \\ C_1 \\ C_2 \\ C_3 \\ C_4 \\ C_5 \end{matrix} : \quad (52)$$

Nevertheless, in all of our numerical simulations the strongly hyperbolic form given by (48) - (50) was used which system was found to be as efficient in accuracy in a number of particular cases as the symmetric hyperbolic system.

V. THE NUMERICAL SCHEME

In our numerical simulations we shall use the simplest possible orthogonal grid based on the $T = \text{const}$ and $R = \text{const}$ 'lines' in the domain $T > T_0$ as it is indicated on Fig.2. The relevant discrete set of grid

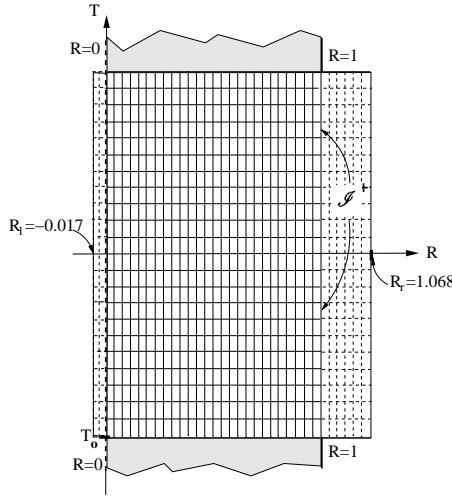


FIG. 2: The domains above the initial data hypersurface $T = T_0$ covered by the simplest possible orthogonal grid are indicated in the applied conformal representations.

points is given as

$$T_1 = T_0 + 1 T; \quad 1 = 0;1; \dots; L_{\max} \quad (53)$$

$$R_i = i R; \quad i = 0;1; \dots; I_{\max}; \quad (54)$$

for some $I_{\max}; L_{\max} \geq N$ fixed numbers and with the relation $T = k R$ for some $k \geq N$. In this setting a function $f = f(T; R)$ will be represented by its values at the indicated grid points, i.e. by $f_i^1 = f(T_1; R_i)$.

In our numerical simulations the total number of spatial grid points was chosen to be an integer power of 2, i.e. 2^N , for some value $N \geq N$. A small fragment of these spatial gridpoints were used to handle the grid boundaries at the origin and beyond future null infinity (see subsection V D for more details). For this purpose we always used $1=2^6$ and $1=2^4$ parts of the spatial gridpoints on the left side of the origin and beyond future null infinity. This means that the formal values of the R -coordinate at these timelike portions of the numerical grid boundaries are $R_1 = \frac{4}{256 \cdot 4 \cdot 16}$

0.017 and $R_r = 1 + \frac{16}{256 \cdot 4 \cdot 16} = 1.068$. Note that the appropriate treatment of the grid boundaries does not require the use of fixed portions of the spatial gridpoints. Nevertheless, we used this simple approach to have a straightforward setting in which we could compare the results of our numerical simulations for various resolutions for the price that only the $236=256$ part of the spatial gridpoints represented points from the original Minkowski spacetime.

A. The time integrator

The time integration of (48) is based on the use of the 'method of lines' in a higher order scheme as it is proposed by Gustafsson *et al* [16]. In particular, we integrate (48), along the constant R_i lines, by making use of a fourth order Runge-Kutta scheme. This is done exactly in the manner as the Runge-Kutta scheme is used to integrate first order ordinary differential equations. Correspondingly, the value of after a 'time step' is determined as

$$\frac{1}{i} = \frac{1}{6} \frac{1}{i} + 2 \frac{1}{(I) i} + 2 \frac{1}{(II) i} + \frac{1}{(III) i} + \frac{1}{(IV) i}; \quad (55)$$

where

$$\frac{1}{(I) i} = T \frac{h}{A_R} @_R \frac{1}{i} + B \frac{1}{T_1; R_i} \frac{1}{i}; \quad (56)$$

$$\begin{aligned} \frac{1}{(II) i} = & T \frac{h}{A_R} @_R \frac{1}{i} + \frac{1}{2} \frac{1}{(I) i} \\ & + B \frac{1}{T_1} + \frac{1}{2} \frac{T; R_i}{T} \frac{1}{i} + \frac{1}{2} \frac{1}{(I) i} \end{aligned} \quad (57)$$

$$\begin{aligned} \frac{1}{(III) i} = & T \frac{h}{A_R} @_R \frac{1}{i} + \frac{1}{2} \frac{1}{(II) i} \\ & + B \frac{1}{T_1} + \frac{1}{2} \frac{T; R_i}{T} \frac{1}{i} + \frac{1}{2} \frac{1}{(II) i} \end{aligned} \quad (58)$$

$$\begin{aligned} \frac{1}{(IV) i} = & T \frac{h}{A_R} @_R \frac{1}{i} + \frac{1}{(III) i} \\ & + B \frac{1}{T_1} + \frac{T; R_i}{T} \frac{1}{i} + \frac{1}{(III) i} \end{aligned} \quad (59)$$

To be able to apply this method of time integration we must calculate R -derivatives of certain functions several times. In this time integration process we approximated these R -derivatives by a symmetric fourth order stencil (see appendix B).

It follows from general considerations [16] that the above described time integration process applied to (48) cannot be stable unless a suitable dissipative term is added to each evaluation of the right hand side of (48). An appropriate dissipative term, relevant for the fourth order Runge-Kutta scheme used here, reads as

$$D = (R)^5 @_R^6; \quad (60)$$

where D is a non-negative constant and the sixth order R -derivatives were evaluated in a symmetric sixth order stencil (see appendix B).

Notice that the use of this dissipative term does not reduce the order of accuracy of the applied finite difference approximation. Moreover, since (48) is an almost everywhere symmetrizable strongly hyperbolic system and all the differential operators are centered it follows from Theorem 6.7.2. of [16] that the applied time integration process is stable provided D is sufficiently large and $k = T = R$ is sufficiently small. Numerical experiments showed us that, for instance, the particular choices $D = 10^{-2}$ and $k = 1/8$ provide

the required stability for the time integration of our evolution equation.

B. The evaluation of the evolving fields at the origin and at future null infinity

Before being able to make the first time step, and later at each of the time levels we have to face the following technical problem. The source term B in (48) contains terms – see the last terms of (45) and (46) – which are given as ratios of expressions vanishing at the origin and at conformal infinity, respectively. The evaluation of these type of expressions generally is a hard numerical problem.

It turned out, however, that the exact value of b_w and b_h is either irrelevant or can be shown to be zero. To see this consider first the evolution of the fields at the origin. By making use of the field equations and assuming that the fields are at least of class C^2 at $R = 0$ we have shown (see (17) - (19)) that in a sufficiently small neighborhood of $R = 0$ the field values w and h must possess the form

$$w = 1 + \hat{w}(T;R) \quad R^2 \quad (61)$$

$$h = \hat{h}(T;R) \quad R^2 \quad \frac{R}{H_1}; \quad (62)$$

where $\hat{w}(T;R)$ and $\hat{h}(T;R)$ are assumed to be sufficiently regular functions of their indicated variables. These relations immediately imply that

$$w(T;0) = 1; \quad (63)$$

$$w_T(T;0) = 0; \quad (64)$$

$$w_R(T;0) = 0; \quad (65)$$

moreover,

$$h(T;0) = 0; \quad (66)$$

$$h_T(T;0) = 0; \quad (67)$$

$$h_R(T;0) = \frac{2H_1}{R}; \quad (68)$$

hold. In other words, the time evolution of our basic variables at the origin is trivial and hence the evaluation of the b_w and b_h is not needed there.

Despite their apparent singular behavior the evaluation of b_w and b_h at $R = 1$ is possible based on the following observations. The first two terms of b_w and b_h are proportional to the conformal factor so they vanish at I^+ . The last terms also vanish there in spite of the presence of the R^2 factors in them since these expressions always contain as a multiplying factor at least one of the massive field variables, either w or, whenever $w \neq 0, h$. These field variables, however, possess the fall off property that $R^n w$ and $R^n h$ for arbitrary positive integer value ($n \geq 2, N$) tend to zero while $R \rightarrow 1$. By making use of this fact, along with the

relation $r = R = 1$, it is straightforward to check that both b_w and b_h must vanish at I^+ . Accordingly, the values of b_w and b_h were kept to be identically zero at $R = 1$ in the numerical simulations.

C. Increasing accuracy

In order to ensure higher order of accuracy we also have applied the following trick. Instead of calculating the time evolution of the variables w and h themselves we determined the evolution of the deviation, $w = w - w_0$ and $h = h - h_0$, of them with respect to certain analytic functions, w_0 and h_0 . In fact, the functions w_0 and h_0 need not necessarily required to be solutions of the field equations although it is favorable to assume that they possess the same type of behavior at $R = 0$ and at I^+ as the functions w and h themselves. This way it was possible to achieve a considerable decrease of the error of our numerical scheme in these critical neighborhoods.

The evolution equations for w and h can be deduced immediately by making use of the assumptions that $w = w + w_0$ and $h = h + h_0$ satisfy (48). The linearity of the involved differential operators yields that

$$\partial_T w = A_R (\partial_R w) + B; \quad (69)$$

where

$$B = B - \partial_T w_0 + A_R (\partial_R h_0) \quad (70)$$

with B being the functional as it is given by (49) but evaluated at the functions $w = w + w_0$ and $h = h + h_0$, moreover, w_0 and h_0 denote the vectors

$$= \begin{pmatrix} 0 & w & 1 \\ B(w)_T & C & \\ B(w)_R & C & \\ h & C & \\ (h)_T & A & \\ (h)_R & A & \end{pmatrix}; \quad w_0 = \begin{pmatrix} 0 & w_0 & 1 \\ \partial_T w_0 & C & \\ \partial_R w_0 & C & \\ h_0 & C & \\ \partial_T h_0 & A & \\ \partial_R h_0 & A & \end{pmatrix}; \quad (71)$$

It is straightforward to verify that in the particular case when w_0 and h_0 are solutions of (39) and (40), i.e. w_0 is a solution of (48),

$$B = B - B_0 = \begin{pmatrix} 0 & (w)_T & 1 \\ b_w & b_{w_0} & C \\ 0 & 0 & C \\ (h)_T & C & \\ b_h & b_{h_0} & A \\ 0 & 0 & A \end{pmatrix}; \quad (72)$$

where b_w and b_h are supposed to be evaluated at the functions $w = w + w_0$ and $h = h + h_0$, respectively. In all our numerical simulations, presented in this paper, w_0 and h_0 were chosen to be the static BPS solution given by (26) and (27) with $C = g = 1$.

D. The treatment of the grid boundaries

In any numerical simulation the appropriate treatment of the grid boundaries requires the most careful considerations. In the case studied here the grid boundary consists of two disjoint parts, the gridpoints representing the origin and the right edge lying in the non-physical spacetime region. It is the evaluation of various derivatives of the dependent variables at these boundaries what desire very careful investigations. The handling of these issues, as they are implemented in our code, are described in the following subsections.

1. The boundary at the origin

As it was already mentioned in Section II A at the origin we can use spherical symmetry and the smoothness of the field variables to gain information about the parity of the relevant functions. This knowledge can then be used to extend these functions onto a *virtually* enlarged grid. In particular, for any function which can be divided into two parts, one of which has a definite parity in coordinate R , while the other part is explicitly known, suitable symmetry transformations can be used to define values of the function at the additional grid points to the left of the word line representing the origin (see Fig. 3). By making use of these values the required number

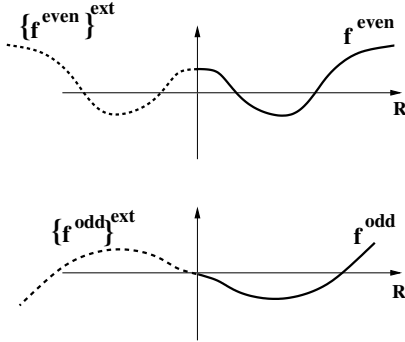


FIG. 3: To the left the extended grid, while to the right the way of extension of functions is indicated for even, f^{even} , and odd, f^{odd} , functions, respectively. In fact, the extensions of these functions are determined by either an axial or a central reflection to the $R = 0$ line or to the ‘central point’ as indicated by the formulas $\text{ff}^{\text{even}} g^{\text{ext}} j_i = f_i^{\text{even}}$ and $\text{ff}^{\text{odd}} g^{\text{ext}} j_i = f_i^{\text{odd}}$, respectively.

of R -derivatives of the applied variables can be determined at $R = 0$. More explicitly, as we will see any function f in our interest can be given as a sum of two functions, $f = f^{\text{dip}} + f^{\text{ext}}$, one of which has a definite parity f^{dip} , being either even or odd function of the R -coordinate, and another explicitly known one f^{ext} . Such a function can be extended, its extension will be denoted by ff^{ext} , to the additional gridpoints

as follows. Suppose, first, that f^{dip} is an even function. Then $f^{\text{even}} = f^{\text{dip}}$ can be extended to the left of $R = 0$ simply by taking the axial reflection, $\text{ff}^{\text{even}} g^{\text{ext}} = (f^{\text{dip}})^{\text{A}R}$, of its graph to the $R = 0$ -axis, defined by the relation $(f^{\text{even}})^{\text{A}R} j_i = f_i^{\text{even}}$. Finally, by making use the fact that f^{ext} is explicitly known and thereby its extension is supposed to be also known (potential singularities at the origin has already been excluded by former assumptions), the extension ff^{ext} of f can be given as $\text{ff}^{\text{ext}} = (f^{\text{dip}})^{\text{A}R} + f^{\text{ext}} g^{\text{ext}}$. A similar process applies whenever f^{dip} is an odd function with the distinction that axial reflection should be replaced by a ‘central reflection’ determined by the relation $(f^{\text{odd}})^{\text{C}R} j_i = f_i^{\text{odd}}$. Thereby the extension of f then can be given as $\text{ff}^{\text{ext}} = (f^{\text{dip}})^{\text{C}R} + f^{\text{ext}} g^{\text{ext}}$.

Turning back to our concrete field variables note first that in the time integration process we need to evaluate R -derivatives of the dependent variables listed as components of the vector valued functions w , w_T , w_R , h , h_T , h_R , see the relation (49). Since w and $h + rH_1$ were found to be even functions of the original r -coordinate, it follows by a straightforward substitution that

$$w = w^{\text{even}}; \quad (73)$$

$$w_T = w_T^{\text{even}}; \quad (74)$$

$$w_R = w_R^{\text{odd}}; \quad (75)$$

$$h = h^{\text{even}} - H_1; \quad (76)$$

$$h_T = h_T^{\text{even}}; \quad (77)$$

$$h_R = h_R^{\text{odd}} - \frac{1+R^2}{2^2} H_1; \quad (78)$$

Thereby the extensions of these functions, to the enlarged grid, yielded by the above described general process are

$$w_i^1 = w_i^1; \quad (79)$$

$$w_T i^1 = w_T i^1; \quad (80)$$

$$w_R i^1 = w_R i^1; \quad (81)$$

$$h_i^1 = h_i^1 + 2H_1 - \frac{1}{i}; \quad (82)$$

$$h_T i^1 = h_T i^1; \quad (83)$$

$$h_R i^1 = h_R i^1 - H_1 - \frac{1+R^2}{2} \frac{1}{i}; \quad (84)$$

Note that whenever we consider the evolution of w with respect to a solution w_0 of (48) – w_0 possesses the same parity properties as the hypothetical solution w itself – thereby the components of w are necessarily even functions of the R -coordinate so their extensions at the origin are straightforward.

2. The grid boundary in the non-physical spacetime

The appropriate treatment of the boundary in the non-physical spacetime requires completely different type of considerations. Clearly, at this part of the boundary there is no way to enlarge the grid based on a suitable combination of certain smoothness and symmetry requirements, as it was possible to be done at the origin. Instead to be able to determine the required number of R -derivatives we used the following two ideas:

First, at the edge and neighboring gridpoints we applied a numerical adaptation what would be called as ‘one sided derivatives’ (see appendix B) in analytic investigations. By making use of these approximations the time integration process can be carried out along the gridlines close to the edge. Second, our problem inherently is a boundary initial value problem (see e.g. [16]). Thus appropriate boundary conditions have to be chosen at the grid boundary to be able to carry on the time integration scheme. There is a considerable freedom in choosing boundary conditions at the edge of the grid. We intended to choose the one which allows waves to travel from the left toward the edge of the grid without being reflected, moreover, which excludes waves coming from beyond this edge toward the direction of the domain of computation. The corresponding restrictions in terms of our basic variables in the static hyperboloidal gauge are

$$w_T = \frac{1}{2} (R + 1)^2 w_R ; \quad (85)$$

$$h_T = \frac{1}{2} (R + 1)^2 h_R ; \quad (86)$$

Numerical experiments justified that this choice did really ensure that the above two requirements were satisfied.

E. Specific choices of parameters in the code

In order to concentrate sufficient number of grid points to the central region where the monopole lives, as well as, to have enough grid points to resolve the expanding shell structures at large radius we have chosen $\gamma = 0.05$ as the parameter included in the coordinate transformation (31) and (32). This specific choice turned out to be appropriate for all the simulations presented in this paper.

For convenience, the total number of spatial grid points was always chosen to be an integer power of 2. Our minimal resolution was $2^8 = 256$, with 4 points in the negative R region and 16 points in the $R > 1$ domain. To preserve the grid point positions when doubling the resolution, in general, we used $4=256 = 1=64$ part of the total spatial grid points for the negative R mirror image points, and $16=256 = 1=16$ part of the total points for the unphysical domain. Keeping

the “size” of the unphysical region above $R > 1$ to be constant is useful when investigating the stability and the convergence of the code in that region, while the unnecessary points in the negative R domain only decrease the speed of the code slightly.

In order to investigate the stability conditions of the numerical code it is helpful to write out the coordinate velocity of the radial null geodesics. Using (37) we get

$$\frac{dR}{dT} = \frac{1}{2} (1 - R)^2 ; \quad (87)$$

where the positive signs correspond to outgoing, the negative signs to ingoing geodesics. The maximal coordinate velocity occurs at null infinity $R = 1$, taking the value 2 for outgoing geodesics. The absolute value of the coordinate velocity of ingoing geodesics is always smaller than 1=2. In principle this would allow any numerical time step T which is smaller than half of the radial step R . However, the evolution equations of the massive field components have an apparent singularity at $R = 1$, where our numerical evolution code was not appropriately stable unless the time step was chosen as small as $T = R=8$.

Choosing the parameter γ in the dissipative term (60) to be $\gamma = 0.01$ stabilize our numerical code without influencing the results significantly even at lower resolutions.

VI. TESTING THE NUMERICAL CODE WITH MASSIVE AND MASSLESS KLEIN-GORDON FIELDS

In order to ascertain the appropriateness of our numerical code we employed it to a physical system for which the time evolution can be established by an independent, certainly more precise method. Because of the linearity of the equations describing the massive Klein-Gordon field its time evolution can be calculated by the Green function method. If the Klein-Gordon field and its derivative are given on a spacelike hypersurface then the field value can be calculated at any point in the future as a sum of two definite (numerical) integrals (for more details see, e.g., [10]). The study of the Klein-Gordon field is especially important, since for several physically important systems, including the magnetic monopole, at large radius the various field components decouple, and behave like independent massive or massless linear Klein-Gordon fields.

In the spherically symmetric case the Klein-Gordon field ϕ satisfies the wave equation

$$\partial_r^2 + \frac{2}{r} \partial_r - \partial_t^2 = m^2 : \quad (88)$$

Introducing the new field variable $z = r$, in the coordinate system $(T;R)$ defined by (31) and (32) the

Klein-Gordon equation takes the form

$$P z = \frac{(R^2 + 1)^2}{4^2} m^2 z ; \quad (89)$$

where the differential operator P is defined in (41). Similarly to the monopole case the equation can be transformed to a system of three first order partial differential equations by introducing the new dependent variables $z_T = \partial_T z$ and $z_R = \partial_R z$.

The initial data on the $T = 0$ hypersurface was chosen as a specification of nonzero time derivative in a localized region superimposed on the vacuum value of the field $z = 0$ as

$$(z_T) = \begin{cases} \frac{h}{c} \exp \frac{d}{(r-a)^2} & \text{if } r \geq [a-b; a+b] \\ 0 & \text{otherwise;} \end{cases} \quad (90)$$

with the constants selected to be $a = 2$, $b = 1.5$, $c = 70$, $d = 10$ and $h = 0.05$ in this section.

First we applied our evolution code to the massive Klein-Gordon field with $m = 1$. On Fig. 4 we compare the field values on a constant T slice obtained with different spatial resolutions to the precise value calculated by the Green function method. The chosen time slice is at $T = 2.4746$, well after the null geodesic emanating from the origin at $T = 0$ has reached null infinity at $T = 1$. It is apparent, that even if the results obtained by the evolution code are not completely satisfactory close to I^+ ($R = 1$) the field values in the central area remain correct for considerably longer time intervals. On Fig. 5 the upper envelope curve for z is shown at a fixed radius, $R = 0.02542$, corresponding to $r = 1.0176$. The frequency of the field oscillations approaches (from above) $m = 1$ in terms of the original time coordinate t , which in the T coordinate corresponds to 20. We can see, that as it may be expected from the behavior of the ingoing null geodesics, the doubling of the resolution increases the time interval where the numerical solution is valid approximately by a factor of two. On Fig. 6 the absolute value of the error at the same constant R radius is shown for several different numerical resolutions. Initially, up to approximately $T = 0.1$, the error values decrease according to the expected fourth order convergence of the code. Later, for $T > 0.3$ the convergence become even faster, approximately fifth order. This behavior is due to dominance of the artificial dissipation term which decreases as $(R)^5$. At later stages a numerical instability arises and the error increases until its absolute value reaches the magnitude of 10^{-16} and the numerical simulation is no longer reliable.

We have also tested our code by applying it to the massless Klein-Gordon field with the same parameters in the initial data (90). With $m = 0$ the Klein-Gordon equation (89) is regular at null infinity $R = 1$ in the compactified representation. On Fig. 7

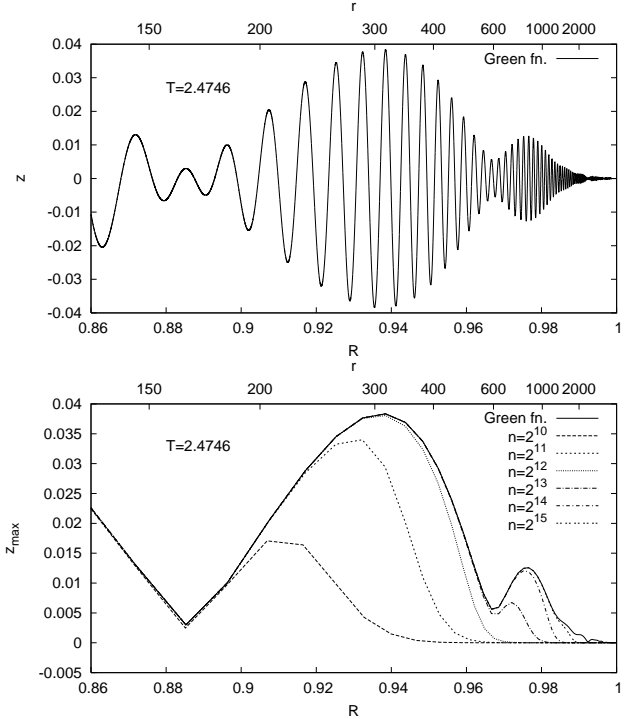


FIG. 4: The behavior of the massive Klein-Gordon field with $m = 1$ at the $T = 2.4746$ slice for large radius is shown. In order to make the expanding shell structures more apparent the function $z = r$ is plotted instead of z .

On the upper graph the oscillations of z as calculated by the Green function method is shown. On the lower graph the upper envelope of the oscillations in z , i.e. the curve connecting the maximum points of the function z , is shown for the Green function calculation, and also for the evolution code corresponding to the indicated spatial resolutions.

we show the rescaled field variable $z = r$ at null infinity as a function of the hyperboloidal time coordinate T obtained with several different numerical resolutions. Since in the massless case information spreads strictly with the velocity of light, the value of z has to be exactly zero before the outgoing light ray from the outer edge of the nonzero initial data, i.e. from $T = 0$ and $r_b = a + b$, reaches null infinity, and has to return to zero again after the ingoing ray from the same point, bouncing through the center reaches null infinity as well. This means that the signal can be nonzero only within the time interval $\frac{2}{c} r_b^2 + 1 < T < \frac{2}{c} r_b^2 + 1 + r_b$ which, after substituting the values of the constants c and r_b , corresponds to the interval $0.8402 < T < 1.1902$. We see that the higher the resolution is the better the numerical simulation can follow the abrupt changes in the magnitude of the field variable. Other feature that can be seen from the figure is that after the signal left the system a numerical noise remains, with a magnitude of about 10^{-16} part of the size of the initial data. The size of this noise remains in this low

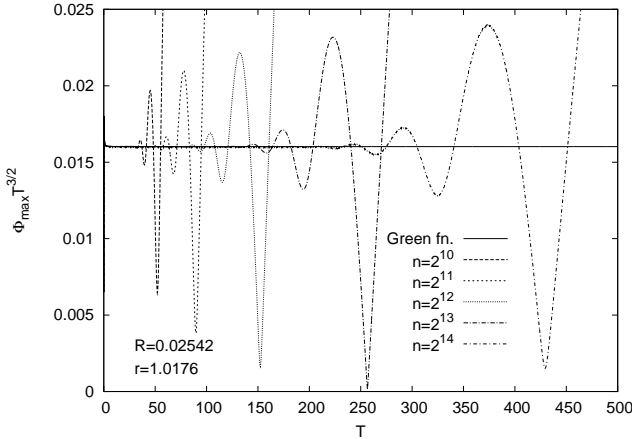


FIG. 5: The upper envelope curve of the oscillations of the Klein-Gordon field at a constant radius close to the center of symmetry. In order to compensate for the fast decay of the field, the envelope of $T^{3/2}$ is plotted, which should tend to a constant value on theoretical grounds. Apart from a short initial period, the envelope of the Green function result is really constant. The envelopes of the functions obtained by the evolution code stay near this constant value for longer and longer times as the number of spatial grid points is increasing.

range for very long time intervals, even for $T = 10^4$.

In order to keep the numerical noise at a low level for very long time intervals a smooth cutoff in the artificial dissipation term has been introduced in the unphysical region $R > 1$. This was necessary because of the incompatibility of the sixth derivative dissipative term with the outgoing boundary condition applied at the outer edge of the grid.

VII. NUMERICAL RESULTS FOR THE TIME EVOLUTION OF MAGNETIC MONOPOLES

A. Choice of initial data

The numerical simulations presented in this paper were carried out in the $\phi = 0$ case, when the Higgs field is massless and the static monopole solution is given by w_s and h_s in (26) and (27). For our numerical simulations we used initial data which consisted of a concentrated spherically symmetric pulse superposed on the static monopole solution. Defining $h_s = r(h_s - H_1)$, at $T = 0$ we choose $(w) = w_s$, $(w_R) = \partial_R w_s$, $(h) = h_s$, $(h_R) = \partial_R h_s$ and

$$\begin{aligned}
 & \frac{8}{8} \frac{h}{h} \frac{i}{i} \\
 & \leq \exp \frac{c}{(r a)^2 b^2} ; \text{ if } r \geq [a - b; a + b]; \\
 (w_T) & = \begin{cases} 0; & \text{otherwise;} \end{cases} \quad (91)
 \end{aligned}$$

In all of the following simulations we take $a = 2$, $b = 1.5$ and $c = 10$, but we choose different amplitudes

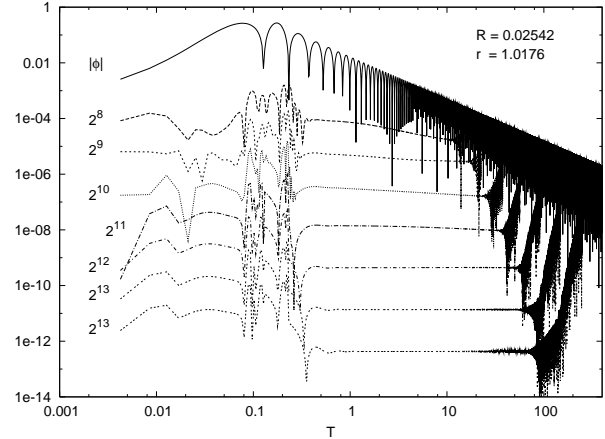


FIG. 6: Logarithmic plot of the absolute error of the value of the massive Klein-Gordon field at constant radius $R = 0.02542$ calculated with several different numerical resolutions corresponding to the indicated number of spatial grid points. The correct absolute value of the field is also plotted in order to show the time intervals where the error is smaller than the actual function value. We note that the downward pointing peaks indicate moments of time where the functions change signature. In order to reduce the complexity of the figure, for each resolution the error is plotted only up to a time where it becomes close to the exact value.

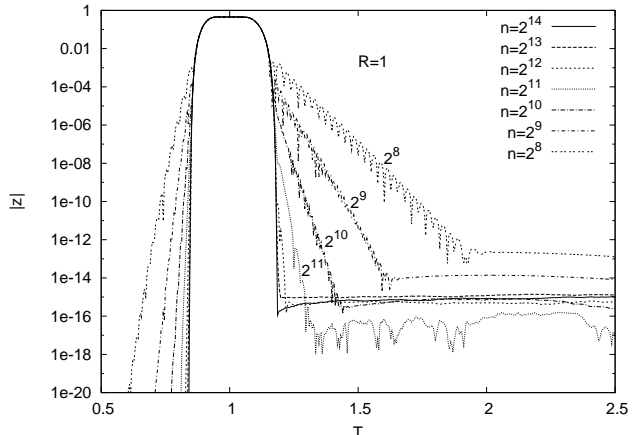


FIG. 7: Time dependence of the absolute value of the rescaled field variable $z = r$ at null infinity $R = 1$ obtained by our numerical code in case of the massless Klein-Gordon field with numerical resolutions corresponding to the indicated number of spatial grid points.

For our basic choice $c = 70$, which is the case discussed in [11], the energy provided by the pulse is about 55.4% of the energy of the background static monopole solution.

B. Constraints

Since we consider the derivatives of w and h as distinct variables the relations $w_R = \partial_R w$ and $h_R = \partial_R h$ represent constraints now. In the analytic setting these relations are preserved by the evolution equations, provided that they hold on the initial surface. A particular test of our numerical code is the monitoring of the violation of these constraints. On Fig. 8 the L^2 norm of the h constraint is presented as a function of time, defined as

$$\|h_R - \partial_R h\|_2^2 = \int_0^{\frac{1}{2}} (h_R - \partial_R h)^2 dR : \quad (92)$$

It can be seen from the figure that for lower resolu-

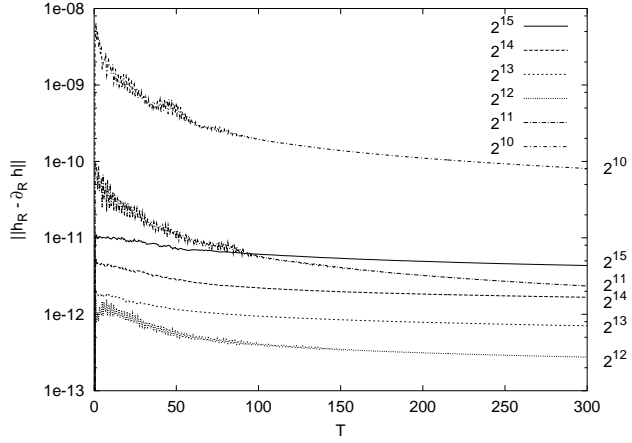


FIG. 8: Time dependence of the h constraint violation for several numerical resolutions corresponding to the indicated number of spatial grid points. The amplitude parameter in the initial data was chosen to be $c = 70$.

tions the error decreases when one increases the number of grid points. However, at higher resolutions, most likely because of rounding errors, the constraint violation becomes higher again. It is also apparent that apart from a short initial period the constraint violation is a decreasing function of time. The time dependence of the w constraint violation is similar to that of h on Fig. 8, only its magnitude is somewhat smaller.

C. Energy balances

To monitor the appropriateness of the applied numerical schema we calculated energy balances for various spacetime domains. In particular, we considered the type of domains shown by Fig. 9 bounded by $T = \text{const.}$ and $R = \text{const.}$ hypersurfaces.

To see how the energy balances can be calculated recall that whenever t^a is a Killing vector field, satisfying the Killing equation $r^{(a} t^{b)} = 0$, the vector field

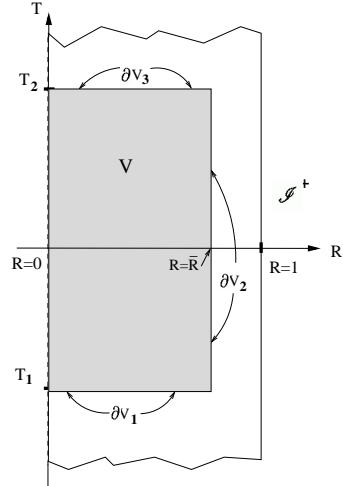


FIG. 9: The boundary $\partial V = \partial V_1 \cup \partial V_2 \cup \partial V_3$ of the shaded spacetime domain, represented by the union of the $T = T_1$, $T = T_2$ and $R = \bar{R}$ hypersurfaces is shown.

$$j^a = T^a b^b \quad (93)$$

is divergence free, i.e.

$$r_a j^a = 0 : \quad (94)$$

Then, by making use of Stokes' theorem we have

$$\int_V r_a j^a = \int_{\partial V} n_a j^a \sim = 0 ; \quad (95)$$

where \sim denotes the 4-volume element while \sim is the 3-volume element induced on the boundary ∂V of V . Note that $\sim_{abc} = n_e e_{abc}$ where n_e is the (outward pointing) unit normal 1-form field on ∂V .

Let us denote by $B(T; R)$ the ball of radius $R = R$ centered at the origin of the $T = T$ ($\leftarrow \text{const}$) hypersurface, moreover, by $C(T_2; T_1; R)$ the portion of the cylindrical hypersurface $R = R$ between the $T = T_1$ and $T = T_2$ hypersurfaces. With these notations the boundaries, as indicated on Fig. 9, ∂V_1 and ∂V_3 are the balls $B(T_1; R)$ and $B(T_2; R)$, while ∂V_2 is the cylinder $C(T_2; T_1; R)$ connecting them. Then the energy contained in a ball $B(T; R)$ can be given as

$$E(T; R) = \int_{B(T; R)} n_a^{(t)} j^a \sim^{(t)} ; \quad (96)$$

where $\sim^{(t)}$ is the volume element on the constant T hypersurface and $n_a^{(t)}$ is its future pointing normal vector. Similarly, the energy transported through the timelike boundary $C(T_2; T_1; R)$ is given as

$$S(T_2; T_1; R) = \int_{C(T_2; T_1; R)} n_a^{(s)} j^a \sim^{(s)} ; \quad (97)$$

where $\sim^{(s)}$ is the volume element on the constant R hypersurface and $n_a^{(s)}$ is its outwards pointing normal vector. Using these notations the energy balance equation (95) takes the form

$$E(T_2;R) - E(T_1;R) + S(T_2;T_1;R) = 0 : \quad (98)$$

Note that while in analytic considerations the l.h.s. of (98) is always identically zero, for any choice of T_2, T_1 and R , in meaningful numerical simulations the corresponding quantity is merely close to zero, i.e. an apparent violation of the energy conservation happens. In fact, the numerical value $N_{\text{vec}}(T_2;T_1;R)$ of the “violation of the energy conservation” associated with a spacetime domain V , which is defined as

$$N_{\text{vec}} = E(T_2;R) - E(T_1;R) + S(T_2;T_1;R); \quad (99)$$

can be used as one of the possible monitorings of the appropriateness of a numerical code.

To evaluate the integrals (96) and (97) we need to determine the volume elements $\sim^{(t)}$ and $\sim^{(s)}$ which can be given as special cases of the relation

$$\sim_{abc} = \frac{q}{\mathcal{B}(4)} \epsilon_{abc} \quad (100)$$

where ϵ_{abc} denotes the Levi-Civita alternating tensor with $\epsilon_{0123} = 1$. To get $\sim^{(t)}$ and $\sim^{(s)}$ consider now the Minkowski spacetime in coordinates $(T;R; ; ;)$ associated with the applied conformal representation. Then the components g of the metric tensor, g_{ab} , and its inverse read as

$$g = \begin{pmatrix} 0 & \frac{2}{R^2} & R & 0 & 0 & 1 \\ \frac{1}{2} \frac{B}{R} & R & 1 & 0 & 0 & C \\ 0 & 0 & R^2 & 0 & 0 & A \\ 0 & 0 & 0 & R^2 \sin^2 & & \end{pmatrix}; \quad (101)$$

and

$$g = \begin{pmatrix} 0 & \frac{4}{(R^2+1)^2} & \frac{4R}{(R^2+1)^2} & 0 & 0 & 1 \\ \frac{B}{2} \frac{4R}{(R^2+1)^2} & \frac{4}{(R^2+1)^2} & \frac{4}{(R^2+1)^2} & 0 & 0 & C \\ 0 & 0 & 0 & \frac{1}{R^2} & 0 & A \\ 0 & 0 & 0 & 0 & \frac{1}{R^2 \sin^2} & \end{pmatrix}; \quad (102)$$

Calculating the determinant $g_{(4)}$ of the spacetime metric we obtain

$$\frac{q}{\mathcal{B}(4)} = \frac{1}{2} R^4 (R^2 + 1) R^2 \sin^2 : \quad (103)$$

The future pointing normal form of $B(T;R)$ has the components $n^{(t)} = (1 = \frac{P}{g^{00}}, 0, 0, 0)$. This implies then that $n^{(t)0} = g^{00} n_0^{(t)} = \frac{P}{g^{00}} = \frac{2}{R^2+1}$, moreover, we have that

$$\sim^{(t)} = \frac{R^2 \sin^2}{3} \epsilon_0 = \frac{q}{\mathcal{B}(t)} \epsilon(dR) \wedge (d) \wedge (d) ; \quad (104)$$

where $h^{(t)}$ is the determinant of the three metric $h_{ab}^{(t)} = \frac{g_{ab}}{P} n_a^{(t)} n_b^{(t)}$ induced by g_{ab} on $B(T;R)$, i.e. $\mathcal{B}(t) j = \frac{R^2 \sin^2}{3}$ on $B(T;R)$. Similarly, the normal of $C(T_2;T_1;R)$, pointing out from the domain V , is $n^{(s)} = (0; 1 = \frac{P}{g^{11}}, 0; 0)$ and thereby $n^{(s)1} = g^{11} n_1^{(s)} = \frac{P}{g^{11}} = \frac{2}{(R^2+1)}$ which implies, in particular, that

$$\sim^{(s)} = \frac{R^2 \sin^2}{2} \epsilon_1 = \frac{q}{\mathcal{B}(s)} j(dT) \wedge (d) \wedge (d) ; \quad (105)$$

where $h^{(s)}$ is the determinant of the induced metric $h_{ab}^{(s)} = g_{ab} + n_a^{(s)} n_b^{(s)}$, and $\mathcal{B}(s) j = \frac{R^2 \sin^2}{2}$.

Taking the above relations into account we get that

$$E(T;R) = 2 \int_0^R (R^2 + 1) \frac{R^2}{4} T^0_0 dR^0 ; \quad (106)$$

$$S(T_2;T_1;R) = 2 \int_{T_1}^{T_2} (R^2 + 1) \frac{R^2}{4} T^1_0 dT ; \quad (107)$$

On Figs. 10 and 11 the time dependence of the violation of the energy conservation $N_{\text{vec}}(0;T;R)$ is shown for numerical runs with various resolutions evolving from initial data with amplitude $c = 70$.

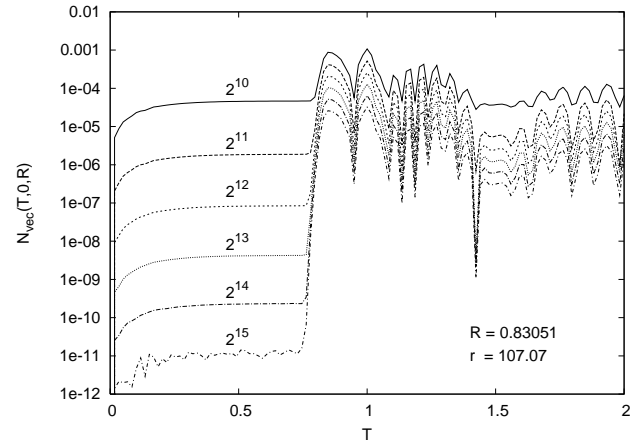


FIG. 10: Initial behavior of the numerical violation of the energy conservation $N_{\text{vec}}(T;0;R)$ for different spatial resolutions is shown. The spacetime domain is bounded by the constant time surfaces $T_1 = 0$ and $T_2 = T$, while the cylindrical boundary is at $R = 0.83051$, corresponding to $r = 107.07$.

It can be seen from these figures that the error in the energy conservation decreases according to expected fourth order convergence during an initial period up to approximately $T = 0.7$ and also later, after $T > 20$. In the intermediate region the conservation violation decreases more slowly. This is possibly due to the highly oscillating character of the fields in that time interval, especially since the energy current integrals

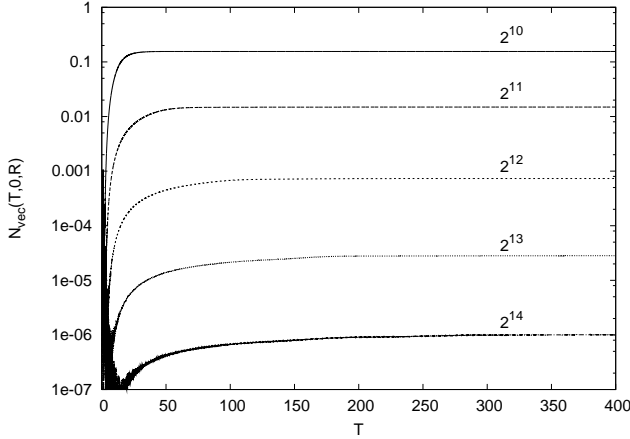


FIG. 11: The time dependence of the violation of the energy conservation $N_{\text{vec}}(T; 0; R = 0.83051)$ for the same numerical simulations as on the previous figure is shown but for a much longer time interval.

were calculated only with a second order convergent method.

The magnitude of the presented constraint violations is really meaningful only if it can be compared to the full energy content. On Fig. 12 the time dependence of the energy content $E(T; R)$ and energy loss $S(T; 0; R)$ is shown for the same spacetime domain as on Figs. 10 and 11. To bring the two curves of the graph into the same range, instead of the total energy $E(T; R)$ the energy difference between $E(T; R)$ and that of the static monopole solution $E_s(R)$ is shown on Figs. 12 and 13. For the chosen initial parameters and radius $R = 0.83051$ the energy of the static background monopole is $E_s(R) = 12.449$, less than double of the energy provided by the initial deformation.

The time dependence of the difference $E(T; R) - E_s(R)$ of the dynamical and static energy functions, $E(T; R)$ and $E_s(R)$, for longer time periods is shown logarithmically on Fig. 13 for increasing numerical resolutions. The convergence of the presented curves provides us a strong indication on how long we can take our numerical results seriously. For the highest resolution used, i.e. that with 2^{15} spatial grid points, the calculation becomes unreliable after $T = 300$. We note that in physical time, i.e. in time measured in mass unites, the time interval $T = 300$ corresponds to $t = 6000$, meanwhile the central monopole performs nearly one thousand oscillations.

D. Energy transfer

In order to distinguish linear and nonlinear effects in the evolution of magnetic monopoles we first present results corresponding to very small initial deformation, with amplitude $c = 0.7$. Then the

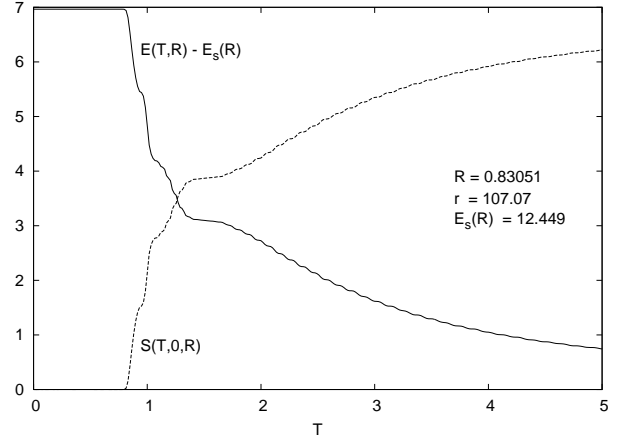


FIG. 12: The solid curve on the graph shows the time dependence of the energy contained inside a radius R on the constant T hypersurface $E(T; R)$ decreased by the energy content of the static monopole, $E_s(R)$. The dashed curve represents the total energy transported through the constant R hypersurface until time T . The sum of these two curves is constant up to errors represented by $N_{\text{vec}}(T; 0; R)$.

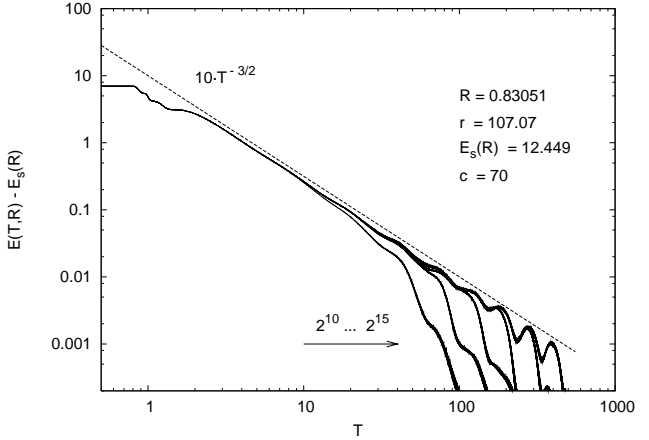


FIG. 13: Time dependence of the extra energy content $E(T; R) - E_s(R)$ for the same system as on the previous figure, but now for longer time periods and with logarithmic axes.

extra energy provided by the initial pulse is only 0.00069783, which is very small compared to the energy of the static monopole, which is 12.566 to five digits precision. On Fig. 14 the time dependence of the extra energy is presented in a ball of radius $R = 0.067797$, which corresponds to $r = 2.7244$. Inside this radius the static background solution contains energy $E_s(R) = 7.0238$, which is about 56 percent of the total energy of the static monopole. For this low energy case, after a short initial period, the energy content starts oscillating around the energy of the static monopole. The time decay of these oscillations is $T^{-5/6}$ to a good approximation. On

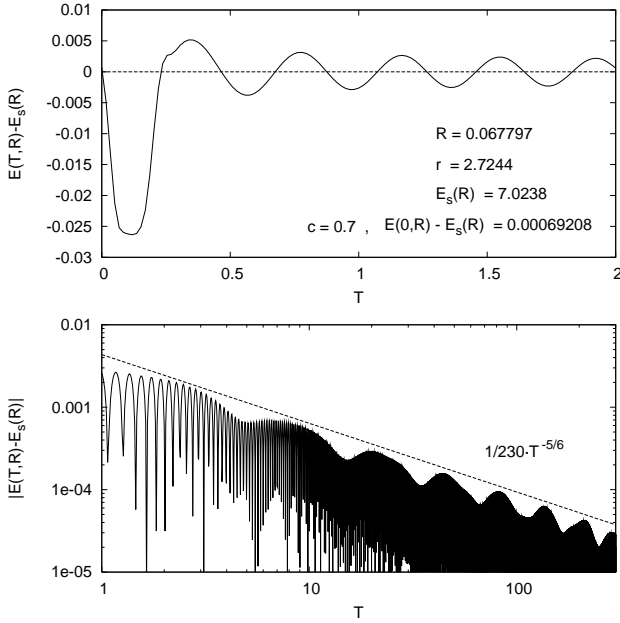


FIG. 14: Extra energy $E(T; R) - E_s(R)$ as a function of time contained inside radius $R = 0.067797$ for an initial and for a longer time period.

Fig. 15 the energy content is presented in a much larger ball, with radius $R = 0.83051$, corresponding to $r = 107.07$. Inside this large radius the energy con-

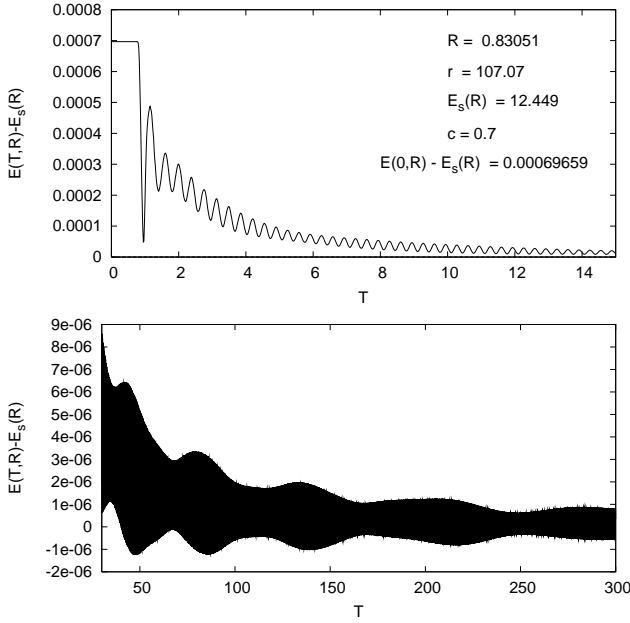


FIG. 15: Extra energy content $E(T; R) - E_s(R)$ for radius $R = 0.83051$ in case of the low energy deformation $c = 0.7$.

tained in the static monopole is 12.449, which is 99 percent of the total static energy. It is apparent that, because the Yang-Mills field is massive, part of the en-

ergy provided by the pulse remains inside this radius for quite a long time. The oscillations of the energy content will be centered around the static value only after about $T > 100$.

On Fig. 16 the energy contained in the same small radius $R = 0.067797$ as the one used at Fig. 14 is shown for a large initial deformation corresponding to $c = 280$. In this case the energy provided by the

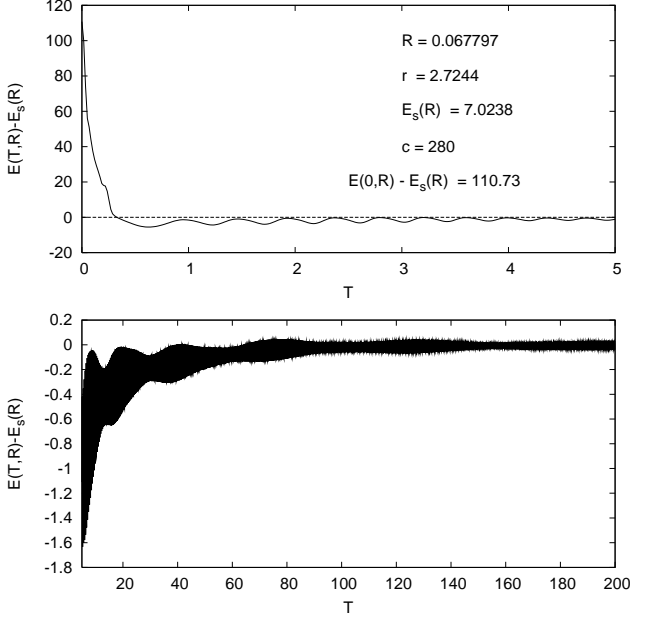


FIG. 16: Extra energy content $E(T; R) - E_s(R)$ for radius $R = 0.067797$ for high energy deformation corresponding to $c = 280$.

pulse is 110.73, which is 15 times more than the energy of the static monopole inside this radius. The main difference compared to the previous case is that the oscillation of the energy is not centered on the static monopole energy anymore. The average value of the energy is below the static value for a very long time period. We interpret this as a nonlinear effect. The expanding initial pulse sweeps out not only the provided extra energy but also a part of the energy of the static monopole. It takes a long time to get back this energy which is stored in the massive Yang-Mills field oscillations at intermediate distances from the monopole. On Fig. 17 the extra energy is shown for the same large initial pulse but for the larger radius, $r = 107.07$. Inside this large radius the energy remains above the static value during the whole time period where our numerical simulation can be considered to be valid.

On Fig. 18 the effect of an extra large initial pulse is presented. In this case the amplitude of the initial pulse was chosen to be $c = 1120$, corresponding to provided energy 1629.6. In this case the initial pulse quickly sweeps out most of the energy of the monopole from the central region. However, after some highly

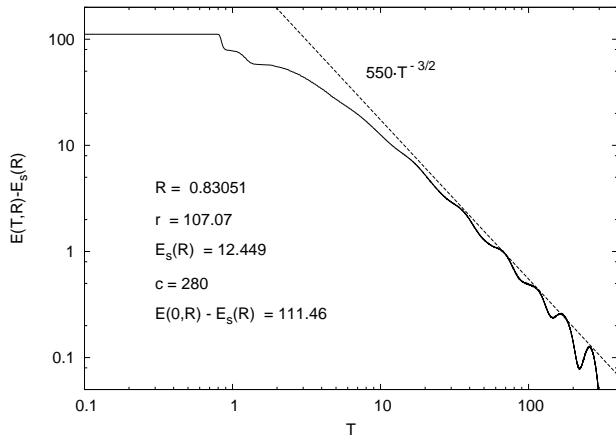


FIG. 17: Extra energy content $E(T;R) - E_s(R)$ for the larger radius, $R = 0.83051$, for high energy deformation corresponding to $c = 280$.

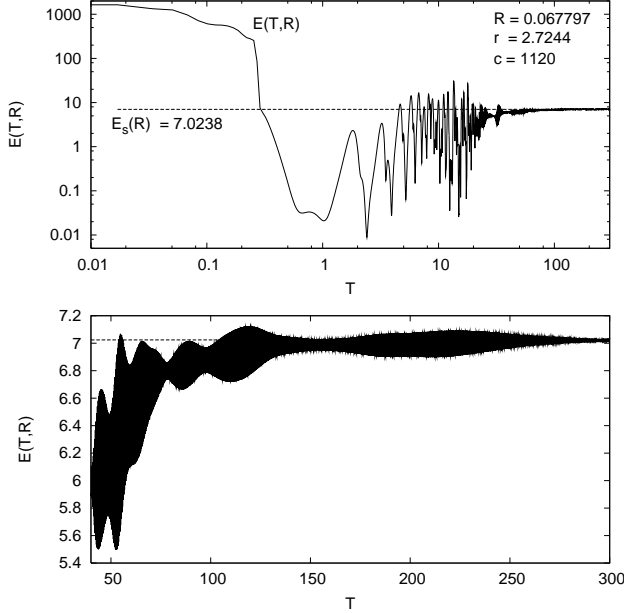


FIG. 18: Full energy content $E(T;R)$ inside radius $R = 0.067797$ for an extra large initial pulse with $c = 1120$.

energetic oscillations, the major part of the monopole energy returns, and the energy content starts to oscillate around a value below that of the static monopole, similarly to the less energetic nonlinear case presented on Fig. 16.

E. The magnetic charge

It is known that in a gauge theory, like the one considered in this paper, by making use of the formal definition applied in Maxwell theory, a conserved magnetic charge can be defined although the yielded

charge is a Lie-algebra-valued quantity. Hence a meaningful definition of magnetic charge requires the use of a gauge independent specification of what is considered to be the “electromagnetic content” of the system.

Historically two main approaches developed. The first one was suggested by 't Hooft [17]. It starts by considering the gauge independent expression [21]

$$F_{ab} = \frac{1}{j} \text{tr}(F_{ab}) + \frac{i}{gj} \text{tr}(\mathbb{D}_a \cdot \mathbb{D}_b); \quad (108)$$

where $j = \text{tr}(\mathbb{D})^{\frac{1}{2}}$. It can be checked that in terms of the variable $A_a = \frac{1}{j} \text{tr}(A_a)$ the above “Maxwell” tensor can be given as

$$F_{ab} = \mathbb{C}_a A_b - \mathbb{C}_b A_a; \quad (109)$$

Note, however, that despite of the elegance of this construction the main drawback is that according to this definition the magnetic charge can reside only at the zeros of the Higgs field, which means that in our case the magnetic charge has to be point-like, it is concentrated to the origin.

According to a general expectation the 't Hooft-Polyakov magnetic monopole has the preferable property of being non-singular in contrast to the Dirac monopole (see e.g. [15]). A proposal, made by Polyakov and Fadaev, fitting to this desire, which will be applied in the rest of this section, is given by the simple relation [2]

$$F_{ab} = \frac{1}{H_0} \text{tr}(F_{ab}); \quad (110)$$

This section is to provide a brief account on the associated definition of the time and location dependent magnetic charge density and the conserved total magnetic charge. Note that in case of the applied minimal dynamical generalization of the static 't Hooft-Polyakov magnetic monopole no electric charge or electric charge density are generated. However, in more generic considerations, involving all the physical degrees of freedom, associated with e.g. the most general spherically symmetric excitations of the BPS magnetic monopole, non-trivial electric charge density appears, although the vanishing of the total electric charge is guaranteed [5].

Analogous to the arguments applied in Maxwell theory the magnetic charge density can be calculated by making use of the magnetic field strength

$$B_a = \frac{1}{2} \epsilon_{abcd} u^b F^{cd} \quad (111)$$

which is defined with respect to a family of observer represented by a timelike unit norm 4-velocity field u^a . The magnetic charge density is given then as the 3-divergence of B_a

$$M = \mathbb{F}^e B_e \quad (112)$$

where \mathcal{E}_a denotes the covariant derivative operator associated with the 3-metric induced on the 3-space "orthogonal" to the 4-velocity field u^a .

To be more specific and precise, let us choose the timelike unit 4-vector field u_a to be everywhere normal to the $T = \text{const}$ hypersurfaces. Then, for the components of u_a

$$u = \frac{1}{\sqrt{g^{TT}}}; 0; 0; 0 \quad (113)$$

holds, while the induced metric on the $T = \text{const}$ hypersurfaces can be given as

$$h_{ab} = g_{ab} - u_a u_b: \quad (114)$$

Notice that for any fixed value of T the vector field u^a coincides with the timelike unit norm $n^{(t)a}$ introduced in the previous section.

Carrying out all the necessary calculations and combining all the above relations we get that

$$B_R = \frac{H}{gR^2} \frac{1}{H_0} (1 - w^2); \quad (115)$$

moreover, the expression of the magnetic charge density Q^M simplifies to the relation

$$Q^M(T;R) = \frac{3}{gH_0 R^2} \frac{\partial H}{\partial R} \frac{(1 - w^2)}{R}; \quad (116)$$

where, in virtue of (28) and (36), the function H stands for the expression $H = h = R + H_0$. It is important to note that in the smooth setting the function $\partial H (1 - w^2) = \partial R$ vanishes up to second order in a small neighborhood of the origin, i.e. there exists a smooth function $\epsilon = \epsilon(T;R)$ so that $\partial H (1 - w^2) = \partial R = \epsilon R^2$. This, however, guarantees that the magnetic charge density Q^M is regular at the centre as it was anticipated.

Let us define, again referring to analogies from Maxwell theory, the magnetic charge associated with a region V in a spacelike hypersurface by the integral

$$Q^M(V) = \int_V \sim^M; \quad (117)$$

where now \sim denotes the 3-volume element of the spacelike hypersurface.

Returning to the previously used specific choice let us choose V to be the ball of radius R centered at the origin on a $T = \text{const}$ hyperboloidal hypersurface, i.e. $V = B(T;R)$. Notice, that according to (114) the components of the 3-volume element \sim takes the form given by the relation (104). Moreover, in virtue of the Stokes' theorem and (112) the magnetic charge associated with the region $B(T;R)$ can be given as a

surface integral on the boundary of $B(T;R)$

$$Q^M(T;R) = \int_{\partial B(T;R)} \mathcal{E}^e B_e \sim = \int_{\partial B(T;R)} e B_e \wedge; \quad (118)$$

where \wedge denotes the outward pointing spacelike unit normal field on the boundary $\partial B(T;R)$ of the region $B(T;R)$, while \wedge is the volume element associated with the induced metric h_{ab} on $\partial B(T;R)$ which is given as

$$h_{ab} = h_{ab} + \partial_a \partial_b: \quad (119)$$

Since the outward pointing unit normal field ∂_a in the considered special case is proportional to $\frac{\partial}{\partial R}$ we have for the components of \wedge that

$$= \frac{1}{h_{RR}}; 0; 0; \quad (120)$$

and hence, also that

$$= \frac{1}{2} \frac{R^2}{0} \frac{0}{R^2 \sin^2}; \quad (121)$$

which leads to the relation

$$\wedge = \frac{R^2 \sin}{2} \wedge_{01} = \frac{q}{j_{(2)} j(d)} \wedge (d); \quad (122)$$

where $j_{(2)}$ is the determinant of the 2-metric h_{ab} , i.e.

$$q \frac{j}{j_{(2)}} = \frac{R^2 \sin}{2}; \quad (123)$$

Combining all the above relations, for the magnetic charge $Q^M(T;R)$ associated with a ball of radius R and centered at the origin on a constant T hypersurface we get

$$\begin{aligned} Q^M(T;R) &= \int_{\partial B(T;R)} \frac{q}{j_{(2)} j(d)} d \wedge d \\ &= \int_0^R \int_{-1}^1 \frac{H(1 - w^2)}{gH_0} \sin d d \\ &= \frac{4}{g} \frac{H}{H_0} 1 - w^2 : \end{aligned} \quad (124)$$

The total magnetic charge, Q^M , associated with the entire of a constant T hyperboloidal hypersurface, can now be given as

$$Q^M = Q^M(T;R = 1); \quad (125)$$

which, in virtue of (124) and since w tends to zero exponentially, while $H = H_0$ tends to one as $R \rightarrow 1$, takes the value

$$Q^M = \frac{4}{g}; \quad (126)$$

Accordingly, the total magnetic charge Q^M is a time independent quantity so that its value coincides with the value of the topological charge of the magnetic monopole.

Acknowledgments

This research was supported in parts by the OTKA grants T034337, TS044665 and the NATO grant PST.CLG.978726. Both of the authors are Bolyai János Research Fellows of the Hungarian Academy of Sciences.

Appendix A

The regularity properties (17) - (19) of the field variables at the origin can be justified by substituting the expansions

$$w(t; r) = \sum_{k=0}^{X^n} \frac{1}{k!} w_k(t) r^k + O_w(r^{n+1}); \quad (A.1)$$

$$H(t; r) = \sum_{k=0}^{X^n} \frac{1}{k!} H_k(t) r^k + O_H(r^{n+1}); \quad (A.2)$$

into the field equations and requiring that the coefficients of the various powers of r vanish identically. The yielded restrictions are

$$w_0(t) = 1 \quad (A.3)$$

$$\partial_r^k w|_{k=0} = w_k(t) = 0; \quad (A.4)$$

for k being odd, and

$$H_0(t) = 0 \quad (A.5)$$

$$\partial_r^k H|_{k=0} = H_k(t) = 0; \quad (A.6)$$

for k being even. It also follows from these relations, along with (A.1) and (A.2), that at the origin the time derivatives $\partial_t w$ and $\partial_t H$ have to vanish throughout the evolution.

Note that part of these restrictions can also be deduced in a different way. In particular, by substituting (A.1) and (A.2) into the tetrad components of the energy momentum tensor we immediately get that these components cannot be finite at the origin unless the relations

$$w_0(t) = 1 \quad (A.7)$$

$$w_1(t) = 0 \quad (A.8)$$

$$H_0(t) = 0 \quad (A.9)$$

are satisfied.

To get the regularity result at future null infinity we need to transform the field equations (15) and (16) into a form suitable to study the asymptotic behavior of the fields at I^+ . Therefore, instead of the standard coordinates $(t; r; ;)$ we apply coordinates $(u; x; ;)$ based on outgoing null geodesic congruences determined by the relations

$$u = t - r \quad \text{and} \quad x = \frac{1}{r}; \quad (A.10)$$

In this frame future null infinity is represented by the $x = 0$ hypersurface, moreover, the field equations (15) and (16) read as

$$x^2 \partial_x^2 w + 2x \partial_x w + 2\partial_x \partial_u w = w - w^2 - 1 + \frac{g^2 H^2}{x^2} \quad (A.11)$$

$$x^3 \partial_x^2 H - 2\partial_u H + 2x \partial_u \partial_x H = xH - 2w^2 + \frac{1}{2x^2} (H^2 - H_0^2) \quad (A.12)$$

Consider now the expansions

$$w = \sum_{k=0}^{X^n} \frac{1}{k!} w_k(u) x^k + O_w(x^{n+1}); \quad (A.13)$$

$$H = \sum_{k=0}^{X^n} \frac{1}{k!} H_k(u) x^k + O_H(x^{n+1}); \quad (A.14)$$

which are valid in a neighborhood of $x = 0$ whenever w and H are at least C^n functions through I^+ , where the notations $w_k(u) = \partial_x^k w(u; x)|_{k=0}$ and $H_k(u) = \partial_x^k H(u; x)|_{k=0}$ have been used. By substituting these expansions into the field equations (A.11) and (A.12) we get the following: Whenever $\epsilon \neq 0$

$$w(u) = 0 \quad (A.15)$$

$$H(u) = H_0 \quad (A.16)$$

$$\partial_x^k w = w_k(u) = 0 \quad (A.17)$$

$$\partial_x^k H = H_k(u) = 0 \quad (A.18)$$

for all $0 < k < n$, i.e., in accordance with the results of Winicour [30], both of the fields decay faster than x^n to their limit values at I^+ . On the other hand, whenever $\epsilon = 0$ and H_1 is non-zero only the vanishing of the x -derivatives of w (up to the order of n) is guaranteed while we get $\partial_u H = 0$, i.e. H_1 is independent of u , there is no restriction for $\partial_u \partial_x H$ and, finally, $\partial_u (\partial_x^k H) = 0$ for $2 \leq k < n$ provided that singular behavior of the field at future (or past) timelike infinite is excluded. Note that the missing of a restriction on $\partial_u \partial_x H$ is in accordance with the following physical picture. The term $\partial_u \partial_x H$ appears in the energy current expression thereby whenever $\epsilon = 0$ the massless Higgs field do transport energy to I^+ . The extent of this energy transport is restricted only by the initial data and the field equation.

Interesting subcases occur (which would deserve further investigations) whenever

$$\epsilon = 0 \quad \text{and} \quad H_1 = 0$$

$$\epsilon \neq 0 \quad \text{and} \quad H_0 \neq 0 \quad \text{but} \quad H_1 = 0$$

$$\epsilon \neq 0 \quad \text{and} \quad H_0 = 0.$$

Then either or both of the fields are massless and there is no restriction on the behavior of the actual massless field or fields at I^+ .

The above considerations shows that a YMH system satisfying reasonable regularity assumptions at I^+ cannot radiate energy to future null infinity unless either $H_0 = 0$ or $H_1 = 0$.

Appendix B

This appendix is to list expressions we applied to represent various numerical R -derivatives in miscellaneous stencils. The expressions below always refer to an arbitrary function f on the I^{th} time slice.

The first and second order R -derivatives relevant for a symmetric fourth order stencil read as

$$\partial_R f_i^1 \equiv \frac{1}{12R} (f_{i+2}^1 + 8f_{i+1}^1 + 8f_{i-1}^1 + f_{i-2}^1) \quad (\text{B.1})$$

and

$$\begin{aligned} \partial_R^2 f_i^1 \equiv & \frac{1}{12(R)^2} (f_{i+2}^1 + 16f_{i+1}^1 + 30f_{i-1}^1 + 16f_{i-2}^1 + f_{i-3}^1) : \end{aligned} \quad (\text{B.2})$$

The first, second and sixth order R -derivatives relevant for a symmetric sixth order stencil were approximated as

$$\begin{aligned} \partial_R f_i^1 \equiv & \frac{1}{60R} (f_{i+3}^1 + 9f_{i+2}^1 + 45f_{i+1}^1 + 45f_{i-1}^1 + 9f_{i-2}^1 + f_{i-3}^1) \\ & + 270f_{i+1}^1 + 490f_i^1 + 270f_{i-1}^1 + 27f_{i-2}^1 + 2f_{i-3}^1 \end{aligned} \quad (\text{B.3})$$

$$\begin{aligned} \partial_R^2 f_i^1 \equiv & \frac{1}{180(R)^2} (2f_{i+3}^1 + 27f_{i+2}^1 + 180f_{i+1}^1 + 490f_i^1 + 270f_{i-1}^1 + 27f_{i-2}^1 + 2f_{i-3}^1) \end{aligned} \quad (\text{B.4})$$

and

$$\begin{aligned} \partial_R^6 f_i^1 \equiv & \frac{1}{(R)^6} (f_{i+3}^1 + 6f_{i+2}^1 + 15f_{i+1}^1 + 20f_i^1 + 15f_{i-1}^1 + 6f_{i-2}^1 + f_{i-3}^1) : \end{aligned} \quad (\text{B.5})$$

We also used a numerical adaptation what would be called as ‘one sided derivatives’ in analytic investigations. The relevant first order ‘left sided derivatives’ are approximated in our fourth order stencil as

$$\begin{aligned} \partial_R f_{\text{Imax}}^1 \equiv & \frac{1}{12R} (3f_{\text{Imax}-4}^1 + 16f_{\text{Imax}-3}^1 + 36f_{\text{Imax}-2}^1 + 48f_{\text{Imax}-1}^1 + 25f_{\text{Imax}}^1) \end{aligned} \quad (\text{B.6})$$

at $i = \text{Imax}$ and as

$$\begin{aligned} \partial_R f_{\text{Imax}-1}^1 \equiv & \frac{1}{12R} (f_{\text{Imax}-4}^1 + 6f_{\text{Imax}-3}^1 + 18f_{\text{Imax}-2}^1 + 10f_{\text{Imax}-1}^1 + 3f_{\text{Imax}}^1) \end{aligned} \quad (\text{B.7})$$

at $i = \text{Imax} - 1$.

The analogous second order ‘left sided derivatives’ read as

$$\begin{aligned} \partial_R^2 f_{\text{Imax}}^1 \equiv & \frac{1}{12(R)^2} (11f_{\text{Imax}-4}^1 + 96f_{\text{Imax}-3}^1 + 114f_{\text{Imax}-2}^1 + 104f_{\text{Imax}-1}^1 + 35f_{\text{Imax}}^1) \end{aligned} \quad (\text{B.8})$$

$$\begin{aligned} \partial_R^2 f_{\text{Imax}-1}^1 \equiv & \frac{1}{12(R)^2} (f_{\text{Imax}-4}^1 + 4f_{\text{Imax}-3}^1 + 6f_{\text{Imax}-2}^1 + 20f_{\text{Imax}-1}^1 + 11f_{\text{Imax}}^1) : \end{aligned} \quad (\text{B.9})$$

The expressions relevant for the sixth order ‘left sided’ derivatives in a sixth order stencil at the spatial gridpoints with indices Imax , $\text{Imax} - 1$ and $\text{Imax} - 3$ do not differ from each other. They are simply yielded by the substitution of $i = \text{Imax} - 3$ into (B.5).

[1] J. Baacke: *Fluctuations and stability of the 't Hooft-Polyakov monopole*, Z. Phys. C. **53**, 399-405 (1999)

[2] E.B. Bogomolny: *Stability of classical Solutions*, Sov. J. Nucl. Phys. **24**, 449 (1976);

[3] J. Burzlaff and N. O'Murchadha: *Global existence of time-dependent Yang-Mills-Higgs monopoles*, Commun. Math. Phys. **105**, 85-98 (1986)

[4] P. Csizmadia: *Testing a new mesh refinement code in the evolution of a spherically symmetric Klein-Gordon field*, Int.J. Mod. Phys. **D 15**, 107 (2006)

[5] P. Csizmadia, Gy. Fodor, I. Rácz and Á. Rusznyák: *The time evolution of generic spherically symmetric magnetic monopoles*, in preparation

[6] R. Courant and D. Hilbert: *Methods of mathematical physics Vol. II.*, New York, Interscience Publishers (1962)

[7] D.M. Eardley and V. Moncrief: *The global existence of Yang-Mills-Higgs fields in 4-dimensional Minkowski spacetime, I. Local existence and smoothness properties*, Commun. Math. Phys. **83**, 171-191 (1982)

[8] D.M. Eardley and V. Moncrief: *The global existence of Yang-Mills-Higgs fields in 4-dimensional Minkowski spacetime, II. Completion of Proof*, Commun. Math. Phys. **83**, 193-212 (1982)

[9] Gy. Fodor, P. Forgács, P. Grandclément, I. Rácz: *Os-*

cillons and Quasi-breathers in the 4 Klein-Gordon model, hep-th/0609023

[10] Gy. Fodor and I. Rácz: *Massive fields tend to form highly oscillating self-similarly expanding shells*, Phys. Rev. D. **68**, 044022 (2003)

[11] Gy. Fodor and I. Rácz: *What does a strongly excited 't Hooft-Polyakov magnetic monopole do?*, Phys. Rev. Lett. **92**, 151801 (2004)

[12] Gy. Fodor and I. Rácz: *Dynamical SU (2) magnetic monopoles*, in *Proc. of the Seventh Hungarian Relativity Workshop, Sárospatak, 2003*, Akadémiai Kiadó, ed. I. Rácz, p. 205-217 (2004)

[13] P. Forgács and N.S. Manton: *Space-time symmetries in gauge theories*, Commun. Math. Phys. **72**, 15-35 (1980)

[14] P. Forgács and M.S. Volkov: *Resonant excitations of the 't Hooft-Polyakov monopole*, Phys. Rev. Lett. **92**, 151802 (2004)

[15] P. Goddard and D. I. Olive: *Magnetic monopoles in gauge field theories*, Rep. Prog. Phys. **41**, 1357-1437 (1978)

[16] B. Gustafsson, H.-O. Kreiss and J. Oliger: *Time dependent problems and difference methods*, (Pure and Applied Mathematics) New York: Wiley (1995)

[17] G. 't Hooft: *Magnetic monopoles in unified gauge theories*, Nucl. Phys. B **79**, 267-284 (1974)

[18] J. Hansen, A. Khokhlov and I. Novikov: *Properties of four numerical schemes applied to a scalar nonlinear scalar wave equation with a GR-type nonlinearity*, Int. J. Mod. Phys. **D13**, 961 (2004)

[19] K. Huang: *Quarks, leptons & gauge fields*, World Scientific Pub., Singapore (1992)

[20] S. Husa: *Numerical relativity with the conformal field equations*, in *Proceedings of the 2001 Spanish Relativity meeting*, eds. L. Fernandez and L. Gonzalez, Springer, Lecture Notes in Physics series, gr-qc/0204057

[21] B. Julia and A. Zee: *Poles with both magnetic and electric charges in non-Abelian gauge theory*, Phys. Rev. D 11, 2227-2232 (1975)

[22] N.S. Manton and P. Sutcliffe: *Topological Solitons*, Cambridge University Press, (2004).

[23] V. Moncrief: *Global existence of solutions of the Yang-Mills equations in Minkowski spacetime*, in *Seminar on new results in nonlinear partial differential equations*, p. 91-100; ed. A.J. Tromba (1987)

[24] V. Moncrief: *Conformally regular ADM evolution equations*, Proc. of the workshop on *Mathematical issues in numerical relativity*, Santa Barbara, (2000),

[25] R. Penrose: *Zero rest-mass fields including gravitation: asymptotic behaviour*, Proc. R. Soc. London, Ser. A, 284, 159-203, (1965).

[26] A.M. Polyakov: *Spectrum of particles in quantum field theory*, JETP Lett. **20**, 430-434 (1974)

[27] M.K. Prasad and C.M. Sommerfield: *Exact classical solution for the 't Hooft Monopole and the Julia-Zee dyon*, Phys. Rev. D. **35**, 760-762 (1975)

[28] V. Rubakov: *Classical Theory of Gauge Fields*, Princeton Univ. Press (2002)

[29] M.S. Volkov and D.V. Gal'tsov *Gravitating Non-Abelian Solitons and Black Holes with Yang-Mills Fields*, Physics Reports, 319, No.1-2, pp.1-83 (1999)

[30] J. Winicour: *Massive fields at null infinity*, J. Math. Phys. **29**, 2117-2121 (1988)